

Magnetically Arrested Disks in Quiescent Black-Hole Binaries: Formation Scenario, Observable Signatures, and Potential PeVatrons

SHIGEO S. KIMURA,^{1,2,*} TAKAHIRO SUDOH,³ KAZUMI KASHIYAMA,^{4,5} AND NORITA KAWANAKA^{6,7}

¹*Frontier Research Institute for Interdisciplinary Sciences, Tohoku University, Sendai 980-8578, Japan*

²*Astronomical Institute, Graduate School of Science, Tohoku University, Sendai 980-8578, Japan*

³*Department of Astronomy, University of Tokyo, Hongo, Tokyo 113-0033, Japan*

⁴*Research Center for the Early Universe, Graduate School of Science, University of Tokyo, Bunkyo-ku, Tokyo 113-0033, Japan*

⁵*Department of Physics, Graduate School of Science, University of Tokyo, Bunkyo-ku, Tokyo 113-0033, Japan*

⁶*Department of Astronomy, Graduate School of Science, Kyoto University, Kitashirakawa Oiwake-cho, Sakyo-ku, Kyoto, 606-8502, Japan*

⁷*Hakubi Center, Kyoto University, Yoshida-honmachi, Sakyo-ku, Kyoto, 606-8501, Japan*

ABSTRACT

We propose magnetically arrested disks (MADs) in quiescent (low luminosity) black-hole (BH) binaries as the origin of the multiwavelength emission, and argue that this class of sources can dominate the cosmic-ray spectrum around the knee. X-ray luminosities of Galactic BH binaries in the quiescent state are far below the Eddington luminosity, and thus, radiatively inefficient accretion flows (RIAFs) are formed in the inner region. Strong thermal and turbulent pressures in RIAFs produce outflows, which can create large-scale poloidal magnetic fields. These fields are carried to the vicinity of the BH by the rapid inflow motion, forming a MAD. Inside the MAD, non-thermal protons and electrons are naturally accelerated by magnetic reconnections or stochastic acceleration by turbulence. Both thermal and non-thermal electrons emit broadband photons via synchrotron emission, which are broadly consistent with the optical and X-ray data of the quiescent BH X-ray binaries. Moreover, protons are accelerated up to PeV energies and diffusively escape from these MADs, which can account for the cosmic-ray intensity around the knee energy.

Keywords: Stellar mass black holes (1611), Low-mass x-ray binary stars (939), Accretion (14), Non-thermal radiation sources (1119), Cosmic ray sources (328)

1. INTRODUCTION

Stellar mass black holes (BHs) in close binaries can emit X-rays through mass accretion from their companion stars. Some emit bright X-rays persistently, whereas the majority are discovered as transient sources (Tetarenko et al. 2016; Corral-Santana et al. 2016). They spend most of their lifetime in the quiescent state, where their luminosities are far below the Eddington luminosity.

Quiescent states of BH X-ray binaries are detected in the radio, infrared/optical, and X-ray bands. The radio emission is widely believed to originate from jets. On the other hand, the origins of the infrared/optical and X-ray signals are still controversial. Hot accre-

tion flow models have been actively discussed since late 90s (Esin et al. 1997; Narayan et al. 1997). However, Chandra and XMM-Newton data indicate that the quiescent spectra are well described by a simple power-law (Pszota et al. 2008), which is in tension with the bumpy spectra predicted by hot accretion flow models (Manmoto et al. 1997; Quataert & Narayan 1999). Jet dominated models are also proposed, where non-thermal electrons accelerated in the jets provide the radio and X-ray signals via synchrotron radiation (Fender et al. 2003; Pszota et al. 2008; Plotkin et al. 2015). However, these models often require additional components, such as an outer optically thick accretion disk or another emission zone in the jet, to explain the infrared and optical data.

In this paper, we propose magnetically arrested disks (MADs) in quiescent BH X-ray binaries (QBXBs) as the origin of the infrared/optical and X-ray emission. A MAD is a strongly magnetized accretion flow where

Corresponding author: Shigeo S. Kimura
shigeo@astr.tohoku.ac.jp

* JSPS Fellow

the magnetic fields affect its dynamics. In MADs, the magnetic energy dissipates through magnetic reconnections (Rowan et al. 2017; Hoshino 2018) and/or turbulent cascades (Howes 2010; Kawazura et al. 2019), which heat up thermal electrons to relativistic energies. They emit infrared/optical photons via cyclosynchrotron radiation. Non-thermal electrons are also accelerated in MADs by magnetic reconnections (Zenitani & Hoshino 2001; Sironi & Spitkovsky 2014) and/or stochastic acceleration by turbulence (Kimura et al. 2016, 2019b; Comisso & Sironi 2018; Zhdankin et al. 2018), and they emit power-law X-rays via synchrotron radiation. MADs can launch a relativistic jet (Tchekhovskoy et al. 2011; McKinney et al. 2012), which is responsible for the radio data. It is believed that MADs are formed in radio galaxies, which is supported by magnetic field estimates based on radio observations (Zamaninasab et al. 2014; Zdziarski et al. 2015). However, the formation mechanism of MADs are not well established yet (see Ressler et al. 2020 for the case of Sgr A*).

MADs can also accelerate non-thermal protons, or cosmic-ray (CR) protons, which can diffusively escape from the MADs. CRs of energies below PeV (“knee”) are believed to be produced in the Milky Way. Supernova remnants are considered to produce Galactic CRs through diffusive shock acceleration (see Schure et al. 2012; Helder et al. 2012, for reviews), and their gamma-ray spectra show that they authentically accelerate protons to GeV - TeV energies (Ackermann et al. 2013; Abeysekara et al. 2020). However, they often show spectral cutoffs or breaks below ~ 10 TeV (Aharonian 2013; Abeysekara et al. 2020), calling into question whether they are capable of generating PeV-scale particles¹. This raised the need for exploring other candidates, which include Sgr A* (HESS Collaboration et al. 2016; Fujita et al. 2017), milli-second pulsars (Guépin et al. 2018), isolated black holes (BHs; Ioka et al. 2017), jets in X-ray binaries (Cooper et al. 2020), pulsar wind nebulae (Ohira et al. 2018), stellar winds from young star clusters (Aharonian et al. 2019), and superbubbles (Bykov 2014). Very recently, Tibet AS γ Collaboration reported discovery of diffuse sub-PeV gamma-rays from the Galactic plane, proving that PeVatrons exist in our Galaxy (Amenomori et al. 2021). Following multi-messenger discussions suggest that PeVatrons can be a population distinct from GeV-TeV CR sources (Liu & Wang 2021; Fang & Murase 2021),

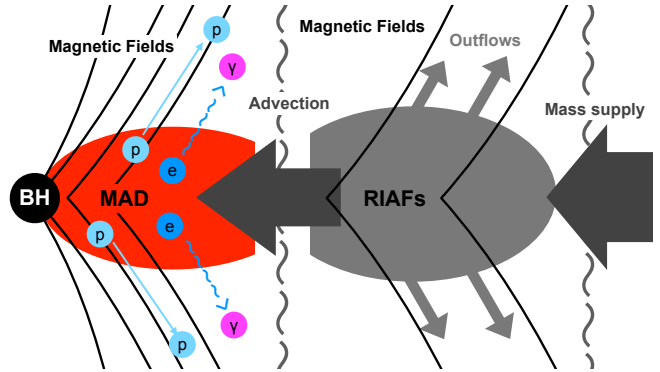


Figure 1. Schematic picture of our QBXB-MAD scenario. In the quiescent state, the standard optically thick disk is truncated at the outer part of the accretion flow. Inside the truncation radius, the accretion flow is in a radiatively inefficient state where outflows are produced. These outflows stretch the magnetic field generated by magneto-rotational instability (MRI) and shear motion, making large-scale poloidal fields. The poloidal fields are advected toward the vicinity of the BH, which results in formation of a MAD. Magnetic reconnections directly heat up thermal electrons and accelerate CR electrons, leading to efficient synchrotron emission that can account for optical and X-ray data. CR protons are also accelerated, and they diffusively escape from the system without losing their energies, possibly providing a dominant contribution to the observed intensity of PeV CRs.

which strengthens the need for other PeVatron candidates. In this paper, we newly add MADs in QBXB (QBXB-MADs) into the list.

This paper is organized as follows. In Section 2, we discuss conditions for the MAD formation in stellar-mass BH binaries and demonstrate that they are fulfilled in the quiescent state. In Section 3, we study emission from thermal and non-thermal electrons in the QBXB-MADs. We focus on a few selected QBXBs that have well-measured multiwavelength spectra. We then show that our QBXB-MAD model is in reasonable agreement with the observed data, which supports our assertion that QBXBs form MADs. In Section 4, we examine the production of CRs in QBXB-MADs. We demonstrate that they can produce PeV-scale protons, potentially dominating the observed CR spectrum around the knee. In Section 5, we discuss implications and outline strategies to test our key assumptions. In Section 6, we present our conclusions. We use the convention of $Q_x = Q/10^x$ in cgs units unless otherwise noted.

2. REALIZATION OF QBXB-MADS

¹ Recently, Albert et al. (2020) and Tibet AS γ Collaboration et al. (2021) independently reported detection of $\gtrsim 100$ TeV photons from a SNR, G106.3+2.7. These findings suggest it as a potential PeVatron.

Figure 1 shows the schematic picture of our scenario. In QBXBs, the mass accretion rate is so low that the accretion flows cannot cool through radiative processes. Then, the optically thick accretion disk should be truncated at an outer radius, and a radiatively inefficient accretion flow (RIAF; Narayan & Yi 1994; Yuan & Narayan 2014) is formed inside the truncation radius (Esin et al. 1997). The accretion flow is turbulent due to magneto-rotational instability (MRI; Balbus & Hawley 1991), and the turbulent viscosity and magnetic torque enable a steady accretion. Thermal, magnetic, and turbulence pressures drive outflows as seen in magnetohydrodynamic (MHD) simulations (Ohsuga & Mineshige 2011; Sądowski et al. 2013; Yuan et al. 2015; Event Horizon Telescope Collaboration et al. 2019). These outflows convert the toroidal magnetic fields generated by the shear motion to the poloidal fields (Liska et al. 2020). The rapid infall motion of the RIAFs can carry these poloidal fields to the inner region. Then, the magnetic flux is accumulated at the vicinity of the BH, leading to the formation of a MAD (Cao 2011). In this section, we discuss the feasibility of our QBXB-MAD scenario based on the current understanding of the plasma and accretion physics. We define a MAD as an accretion flow with $\beta \lesssim 1$, where β is the plasma beta. Here, we ignore the magnetic flux carried from the companion star. If we take it into account, MADs are more likely to be formed. In this sense, our estimates in this section is conservative.

In RIAFs, the matter cannot cool within the infall timescale, which results in a proton temperature comparable to the virial temperature. RIAFs are geometrically thick because of the strong thermal pressure. The thick geometry allows a large turbulent eddy, which leads to a large turbulent viscosity. Then, the angular momentum transport is efficient, resulting in a radial motion faster than the standard thin disk. Since RIAFs produce outflows, the mass accretion rate can depend on the distance from the BH, R , and written as $\dot{M}(R) = (R/R_{\text{trn}})^{s_w} \dot{M}_o$, where R_{trn} is the truncation radius, \dot{M}_o is the mass accretion rate at $R = R_{\text{trn}}$, and s_w is a parameter that describes the outflow efficiency (Blandford & Begelman 1999). The radial velocity, sound velocity, and density in RIAFs can be analytically estimated to be (see Kimura et al. 2019a; Kimura et al. 2020, for parameter sets for active galactic nuclei (AGN))

$$V_R \approx \frac{1}{2} \alpha V_K \simeq 4.7 \times 10^7 \alpha_{-0.5} \mathcal{R}_4^{-1/2} \text{ cm s}^{-1}, \quad (1)$$

$$C_s \approx \frac{1}{2} V_K \simeq 1.5 \times 10^8 \mathcal{R}_4^{-1/2} \text{ cm s}^{-1}, \quad (2)$$

$$N_p \approx \frac{\dot{M}(R)}{4\pi R H V_R m_p} \quad (3)$$

$$\simeq 1.3 \times 10^{11} \left(\frac{\dot{m}(R)}{0.01} \right) M_1^{-1} \mathcal{R}_4^{-3/2} \alpha_{-0.5}^{-1} \text{ cm}^{-3},$$

where M is the BH mass, $M_1 = M/(10M_\odot)$, $V_K = \sqrt{GM/R}$ is the Keplerian velocity, α is the viscous parameter (Shakura & Sunyaev 1973), $H \approx (C_s/V_K)R \approx R/2$ is the scale height, $\dot{m}(R) = \dot{M}(R)c^2/L_{\text{Edd}}$, $\mathcal{R} = R/R_G$, L_{Edd} is the Eddington luminosity, m_p is the proton mass, and $R_G = GM/c^2$ is the gravitational radius. The pre-factors in V_R and C_s are determined so that the quantities are consistent with recent MHD simulations (Ohsuga & Mineshige 2011; Kimura et al. 2019b).

Electrons and protons in RIAFs are thermally decoupled because of a long relaxation timescale. Electrons in collisionless plasma can receive a significant fraction of the dissipation energy by magnetic reconnections and turbulence cascades (Rowan et al. 2017; Kawazura et al. 2019), and they do not efficiently cool if they are non-relativistic. Thus, electrons are expected to be close to the virial temperatures for $R \gtrsim (m_p/m_e)R_G$, where m_e is the electron mass. On the other hand, electrons become relativistic for the inner region and efficiently cool via synchrotron and Comptonization processes (e.g., Narayan et al. 1995; Manmoto et al. 1997; Kimura et al. 2015). Then, the electron temperature is almost independent of \mathcal{R} and frozen to the mildly relativistic regime (e.g., Narayan & Yi 1995; Kimura et al. 2020).

The truncation radius can be estimated by balancing the accretion timescale and proton cooling timescales. The accretion timescale for a RIAF can be estimated to be

$$t_{\text{fall}} \approx \frac{R}{V_R} \simeq 3.1 \times 10^2 \mathcal{R}_4^{3/2} M_1 \alpha_{-0.5}^{-1} \text{ sec}. \quad (4)$$

Thermal protons mainly lose their energies via Coulomb scattering with electrons. The energy loss timescale is given by

$$t_{pe} = \frac{\sqrt{2\pi}}{2N_p \sigma_T c \ln \Lambda} \frac{m_p}{m_e} \theta_e^{3/2}, \quad (5)$$

where σ_T is the Thomson cross section, $\ln \Lambda \sim 20$ is the Coulomb logarithm, and $\theta_e = k_B T_e / (m_e c^2)$ is the normalized electron temperature. To obtain Equation (5), we assume non-relativistic limit and $\theta_e > \theta_p$, where $\theta_p = k_B T_p / (m_p c^2)$ is the normalized proton temperature. The latter condition is always satisfied for RIAFs, while electrons can be relativistic at $R \lesssim (m_p/m_e)R_G$. The cooling timescale of thermal electrons is shorter than the Coulomb interaction timescales in RIAFs, and thus, Equation (5) is regarded as the cooling timescale of RIAF plasma. In cases with a sufficiently low \dot{m} , the

temperatures in the outer region can be approximated as $kT_e \sim kT_p \sim m_p C_s^2$, i.e., $\theta_e \approx (m_p/m_e)(V_K/c)^2/4$, which leads to

$$t_{pe} \simeq 4.4 \times 10^2 \left(\frac{\dot{m}(R)}{0.01} \right)^{-1} M_1 \alpha_{-0.5} \text{ sec.} \quad (6)$$

Equating t_{pe} and t_{fall} , we estimate the truncation radius to be

$$\mathcal{R}_{\text{trn}} \approx 1.3 \times 10^4 \alpha_{-0.5}^{4/3} \dot{m}_{o,-2}^{-2/3}, \quad (7)$$

where $\dot{m}_o = \dot{M}_o c^2 / L_{\text{Edd}}$. Therefore, the truncation radius can be larger than $(m_p/m_e)R_G$ when $\dot{m}_o \lesssim 0.1 \alpha_{-0.5}^2$, which justifies our assumption of $kT_e \sim kT_p$. Such a large truncation radius is supported by the spectroscopic observation of QBXBs. The widths of double-peak emission lines in the quiescent state indicate a circular motion of $\sim 10^3 \text{ km s}^{-1}$, which infer a thin disk truncated at $R_{\text{trn}} \sim 10^4 R_G$ (Orosz et al. 1994; McClintock et al. 2003).

In RIAFs, strong poloidal fields can be generated even from a small seed field. We estimate the poloidal field strength at the wind launching region. Non-linear growth of MRI creates the magnetic field of $\beta \approx 8\pi m_p N_p C_s^2 / B^2 \sim 10 - 100$, which is dominated by the toroidal field (Hawley et al. 2013; Kimura et al. 2019b). Thermal and magnetic pressures drive outflows (Ohsuga & Mineshige 2011; Sądowski et al. 2013; Yuan et al. 2015; Event Horizon Telescope Collaboration et al. 2019), which convert the toroidal magnetic fields to the poloidal fields. The poloidal magnetic field is as strong as 30-40% of the total magnetic field based on MHD simulations (Hawley et al. 2013; Kimura et al. 2016, 2019b), although these values contain the turbulent component. Assuming that the global poloidal field strength is comparable to the turbulent poloidal fields, we estimate the plasma beta by the global poloidal fields to be $\beta_p = 8\pi m_p N_p C_s^2 / B_p^2 \sim 10^3 - 10^4$, where B_p is the poloidal field strength.

The rapid infall motion of RIAFs can carry these poloidal fields to the inner region. If we assume the magnetic flux freezing, the poloidal field and gas pressure scale as $B_p \propto R^{-2}$ and $N_p C_s^2 \propto R^{-5/2+s_w}$, respectively. Thus, the poloidal plasma beta scales as $R^{3/2+s_w}$. Then, the accreting plasma of $\beta_{p,o}$ at $R \sim R_{\text{trn}}$ would become $\beta_{p,i} \sim (R_G/R_{\text{trn}})^{3/2+s_w} \beta_{p,o}$ at $R \sim R_G$. For $\beta_{p,o} \sim 10^4$ and $R_{\text{trn}} \sim 10^4 R_G$, we obtain $\beta_{p,i} \sim 10^{-3}$ for $s_w \sim 0.25$. We note that $s_w \sim 0.2 - 0.3$ is often used when ones try to fit the broadband spectra in low-Eddington objects (Yuan et al. 2003; Nemmen et al. 2014).

Such a strongly magnetized flow is unlikely to be realized, because the strong magnetic fields halt the accretion. In reality, some mechanisms, such as mag-

netic Rayleigh-Taylor instability (MRTI), should prevent the enhancement of the poloidal field by disturbing the poloidal field locally. This will maintain the moderately strong magnetic field of $\beta \sim 0.1 - 1$, and form a MAD where the magnetic flux threading the horizon is equal to the saturation value (Tchekhovskoy et al. 2011; Narayan et al. 2012). Indeed, analytic modelings of magnetic fluxes suggest that rapid inward motion of RIAFs can result in accumulation of poloidal magnetic fields at the vicinity of the BH (Cao 2011). Also, magnetic flux accumulation by advection is discussed in the context of the jetted tidal disruption event (Tchekhovskoy et al. 2014). The high-resolution and long-term general relativistic (GR) MHD simulations support the idea that the outflows create poloidal fields from toroidal fields and a MAD is eventually formed by advection of the poloidal fields (Liska et al. 2020). In light of these considerations, we conclude that Galactic X-ray binaries in their quiescent state very likely host MADs.

We cautiously note that our argument is applicable only for highly sub-Eddington systems, e.g., quiescent states in X-ray binaries. RIAFs with relatively high mass accretion rates ($\dot{m}_o \gtrsim 0.01$) are expected in low-hard states, and the truncation radius in this state should be smaller (Esin et al. 1997). In this situation, MADs are unlikely to be formed (see Section 5 for detail). Also, some long-term GRMHD simulations do not arrive at the MAD state (Narayan et al. 2012; White et al. 2020). This may indicate that our scenario may not be always applicable even for highly sub-Eddington systems. Currently, the exact condition of MAD formation is still unclear, and further investigation is necessary in order to understand whether they are ubiquitous in highly sub-Eddington systems.

3. PHOTON SPECTRA FROM QBXB-MADS

MADs dissipate their magnetic energy through magnetic reconnections and/or turbulence cascades, which heat up the thermal plasma and accelerate CR protons and electrons. We calculate the photon spectra from the QBXB-MADs based on the formalism in Kimura & Toma (2020), where one-zone and steady state approximations are utilized. We consider an accreting plasma² of size $R = \mathcal{R}R_G = \mathcal{R}GM/c^2 \simeq 1.5 \times 10^7 \mathcal{R}_1 M_1 \text{ cm}$ with the mass accretion rate $\dot{M} = \dot{m} L_{\text{Edd}}/c^2 \simeq 2.2 \times 10^{-12} M_\odot \text{ yr}^{-1} \dot{m}_{-4} M_1$. To estimate

² We consider accretion rate at $R = \mathcal{R}R_G$, which should be lower than \dot{M}_o in Section 2 because $\dot{M}(R) \approx \dot{M}_o (R/R_{\text{trn}})^{s_w}$ with $s_w > 0$. s_w , R_{trn} , and \dot{M}_o do not appear explicitly in our calculations of the emission from the MAD.

Table 1. List of model parameters and physical quantities. The references for BH masses and distances are Cantrell et al. (2010); Gandhi et al. (2019) for A0620-00, Khargharia et al. (2010); Miller-Jones et al. (2009) for V404 Cyg, and Khargharia et al. (2013); Gelino et al. (2006) for XTE J1118+480.

Shared Parameters					
α	\mathcal{R}	ϵ_{dis}	η	ϵ_{NT}	s_{inj}
0.3	10	0.15	5	0.33	1.3
Parameters for individual BHs					
Name	$M [M_{\odot}]$	$\dot{m} [10^{-4}]$	β	$d_L [\text{kpc}]$	
A0620-00	6.6	1.0	0.40	1.7	
V404 Cyg	9.0	2.0	0.50	2.4	
XTE J1118+480	7.5	0.10	0.10	1.7	
Hypothetical ^a	10	0.1 – 100	0.1 – 0.5	2 – 8	

^a Cases shown in Figure 3, Figure 4, and Figure 5

physical quantities in MADs, we use the analytic prescription for RIAFs with a parameter set appropriate for MADs. The radial velocity and magnetic field of the QBXB-MAD are written as

$$V_R \simeq 1.5 \times 10^9 \mathcal{R}_1^{-1/2} \alpha_{-0.5} \text{ cm s}^{-1} \quad (8)$$

$$B \approx \sqrt{\frac{8\pi m_p N_p C_s^2}{\beta}} \quad (9)$$

$$\simeq 6.2 \times 10^5 \mathcal{R}_1^{-5/4} \dot{m}_{-4}^{1/2} M_1^{-1/2} \alpha_{-0.5}^{-1/2} \beta_{-1}^{-1/2} \text{ G},$$

where we provide β as a parameter. These analytic expressions are in rough agreement with the results of GR MHD simulations of MADs (Narayan et al. 2012; White et al. 2019).

The energy dissipation rate can be parameterized as $Q_{\text{dis}} \approx \epsilon_{\text{dis}} \dot{m} L_{\text{Edd}}$, where ϵ_{dis} is the dissipation parameter. Based on PIC simulations, the energy partition between protons and electrons are given by $Q_p/Q_e \approx (m_p/m_e)^{1/4} (T_p/T_e)^{1/4}$ (Hoshino 2018). Introducing the non-thermal particle production efficiency, ϵ_{NT} , we write the CR proton and electron luminosities as $L_{p,\text{CR}} = \epsilon_{\text{NT}} \epsilon_{\text{dis}} \dot{m} L_{\text{Edd}}$ and $L_{e,\text{CR}} = \epsilon_{\text{NT}} (Q_e/Q_p) \epsilon_{\text{dis}} \dot{m} L_{\text{Edd}}$, respectively. The heating rate of thermal electrons is then given by $L_{e,\text{thrm}} = (1 - \epsilon_{\text{NT}}) (Q_e/Q_p) \epsilon_{\text{dis}} \dot{m} L_{\text{Edd}}$. The proton temperature can be estimated as $k_B T_p \approx m_p C_s^2$ (see the next paragraph for the electron temperature). We consider 4 components: thermal electrons, CR electrons, CR protons, and secondary electron-positron pairs.

First, we describe emissions from the thermal component. The thermal electrons emit photons via cyclosynchrotron, bremsstrahlung, and Comptonization processes, whose emissivities strongly depend on the electron temperature. We calculate the photon spectra by

the method given in Appendix of Kimura et al. (2015), except for the fitting formula of the thermal cyclosynchrotron emission; we utilize a formula for sub- and mildly relativistic electrons given in Mahadevan et al. (1996). We compute the cooling rate by integrating the emitted photon spectrum, and obtain the electron temperature by balancing the cooling rate with the heating rate iteratively.

Next, we explain the CR components. We solve the transport equations for the CR protons and electrons:

$$-\frac{d}{dE_i} \left(\frac{E_i N_{E_i}}{t_{i,\text{cool}}} \right) = -\frac{N_{E_i}}{t_{\text{esc}}} + \dot{N}_{E_i,\text{inj}}, \quad (10)$$

where $i = e, p$ indicates the particle species, E_i is the particle energy, N_{E_i} is the number spectrum, $\dot{N}_{E_i,\text{inj}}$ is the injection term, and $t_{i,\text{cool}}$ and t_{esc} ³ are the cooling and escape timescales, respectively. We use a single power-law injection function with an index s_{inj} and exponential cutoff at $E_{i,\text{cut}}$, i.e., $\dot{N}_{E_i,\text{inj}} \propto (E_i/E_{i,\text{cut}})^{-s_{\text{inj}}} \exp(-E_i/E_{i,\text{cut}})$, normalizing it by $L_{i,\text{CR}} = \int \dot{N}_{E_i,\text{inj}} E_i dE_i$.

The cutoff energy is obtained by balancing the acceleration and loss timescales. The acceleration timescale is given by $t_{i,\text{acc}} \approx \eta r_{i,L} / (c \beta_A^2)$, where $\beta_A = B / \sqrt{4\pi N_p m_p c^2}$ is the Alfvén velocity in unit of c , $\eta r_{i,L}$ is the particle mean-free path, $r_{i,L} = E_i / (eB)$ is the Larmor radius, and η is the acceleration efficiency parameter. The loss timescale is $t_{i,\text{loss}}^{-1} = t_{i,\text{cool}}^{-1} + t_{\text{esc}}^{-1}$. We consider advective (infall to the BH) and diffusive escapes. The advective and diffusive escape timescales are given by $t_{\text{adv}} = R/V_R$ and $t_{\text{diff}} = 3R^2 / (\eta r_{i,L} c)$, respectively, and the escape timescale is given by $t_{\text{esc}}^{-1} = t_{\text{adv}}^{-1} + t_{\text{diff}}^{-1}$. As the cooling process of CR electrons, we only consider synchrotron emission, $t_{e,\text{cool}} = t_{e,\text{syn}}$, where $t_{e,\text{syn}}$ is the synchrotron cooling timescale for electrons, because other processes are negligible⁴. Regarding the CR protons, we consider pp inelastic collisions ($p + p \rightarrow p + p(n) + \pi$), photomeson production ($p + \gamma \rightarrow p(n) + \pi$), Bethe-Heitler ($p + \gamma \rightarrow p + e^+ + e^-$), and proton synchrotron processes. We write the proton cooling timescale as $t_{p,\text{cool}}^{-1} = t_{pp}^{-1} + t_{p\gamma}^{-1} + t_{\text{BH}}^{-1} + t_{p,\text{syn}}^{-1}$, where t_{pp} , $t_{p\gamma}$, t_{BH} , and $t_{p,\text{syn}}$ are the cooling timescales by pp inelastic collision, pho-

³ The value of t_{esc} for CR protons and CR electrons for a given energy are the same, so we omit i from t_{esc} .

⁴ We can ignore inverse Compton scattering and bremsstrahlung emissions by CR electrons in QBXB-MADs. The magnetic field energy density is higher than the photon energy density by about two orders of magnitude, which enables us to ignore the inverse Compton emission. The plasma density in the QBXB-MAD is so low that the bremsstrahlung emission provides a negligible contribution.

meson production, Bethe-Heitler, and proton synchrotron processes, respectively. The expressions for them are given in Kimura et al. (2019a), and we appropriately take into account the energy dependent cross sections (Stepney & Guilbert 1983; Chodorowski et al. 1992; Murase & Nagataki 2006; Kafexhiu et al. 2014). In the range of our interest, the proton synchrotron process dominates over the other three⁵. The secondary electron-positron pairs are produced via Bethe-Heitler processes, decay of pions, and two-photon pair productions. They emit gamma-rays via synchrotron emission. Although we approximately take into account the emission by secondary electron-positron pairs, their contributions to the resulting photon spectra are subdominant in the range of our interest.

Figure 2 indicates broadband photon spectra from the QBXB-MADs for three BH X-ray binaries, whose parameters are given in Table 1. We select these objects because the qualities of their data sets in the quiescent states are better than others. Our scenario is in broad agreement with the optical/infrared and X-ray data. Thermal electrons emit optical photons by cyclosynchrotron emission. We find that MADs with $\dot{m} \gtrsim 10^{-5}$ are still optically thick for synchrotron-self absorption at the synchrotron characteristic frequency. In this case, the peak frequency of the synchrotron spectrum is estimated to be (Mahadevan 1997; Kimura et al. 2020)

$$E_{\text{syn,abs}} \approx \frac{3x_M e B \theta_e^2 h_p}{4\pi m_e c} \simeq 1.1 B_{5.5} \theta_e^2 \left(\frac{x_M}{200} \right) \text{ eV}, \quad (11)$$

where $x_M = E_{\text{syn,abs}}/E_{\text{syn,pk}} \approx 2.2 \times 10^3 \dot{m}^{1/4}$ is the conversion factor from the synchrotron frequency, $E_{\text{syn,pk}} = 3\theta_e^2 h_p e B / (4\pi m_e c)$, to the spectral peak, $E_{\text{syn,abs}}$ (Mahadevan 1997), and h_p is the Planck constant. This value is in agreement with the peak energy of the optical non-stellar component. The Thomson optical depth of QBXB-MADs is too low to emit X-rays by Comptonization, but CR electrons in QBXB-MADs can emit high-energy photons up to the MeV range. Equating $t_{e,\text{cool}}$ to t_{fall} and t_{acc} , we estimate the cooling and cutoff energies to be $E_{\gamma,\text{cl}} \approx h_p e B \gamma_{e,\text{cl}}^2 / (2\pi m_e c) \sim 3.7 \times 10^{-3} B_{5.5} \gamma_{e,\text{cl}}^2$ eV and $E_{\gamma,\text{cut}} \approx 3e^2 h_p \beta_A^2 / (m_e c \sigma_T \eta) \sim 15(\beta_A/0.7)^2 (\eta/5)^{-1}$ MeV, respectively, where $\gamma_{e,\text{cl}} \approx \max(1, 6\pi m_e c V_R / (\sigma_T B^2 R))$ is the electron Lorentz factor at the cooling break. In our parameter choice,

⁵ pp inelastic collisions and photomeson production processes can produce high-energy neutrinos, and thus, these are relevant in view of multi-messenger astrophysics. However, we found that QBXB-MADs are too faint to be detected by high-energy neutrino telescopes near future.

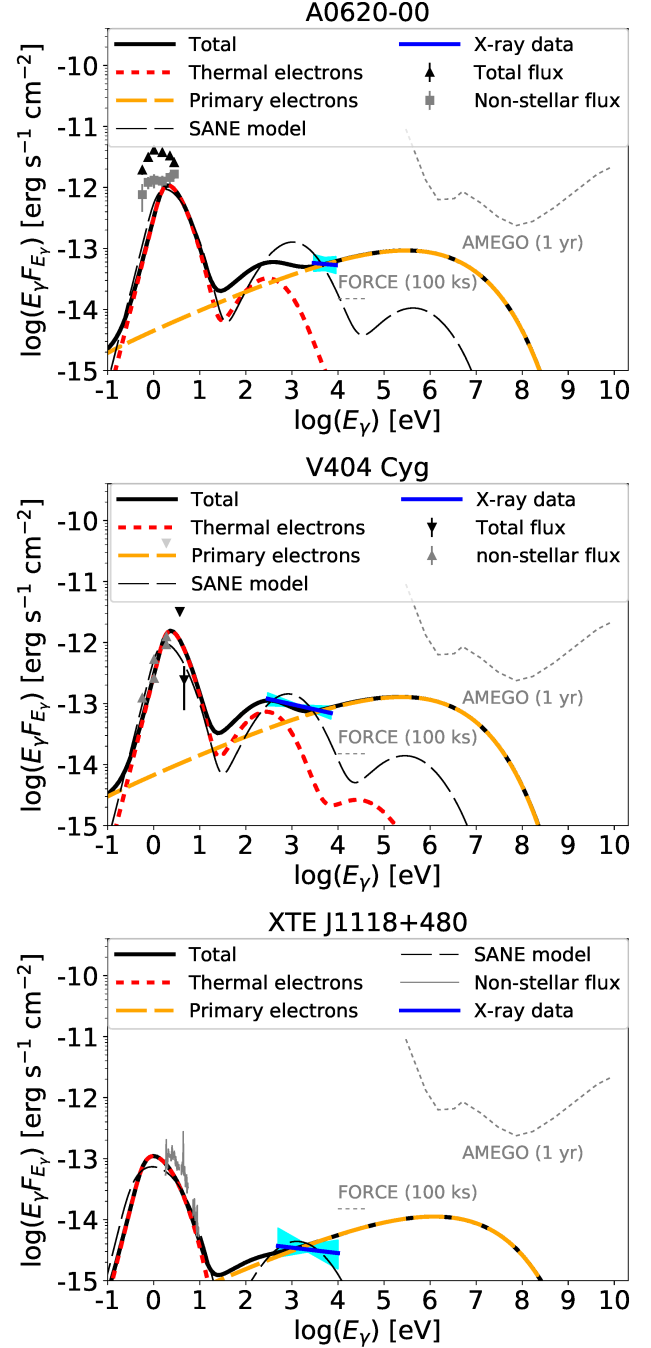


Figure 2. Broadband spectra for well-known BH X-ray binaries, A0620-00 (top), V404 Cyg (middle), and XTE J1118-480 (bottom), in quiescent states. Thick lines are photon spectra by the MAD scenario (this study) and the thin-dashed lines are ones for a weak magnetic field scenario (SANE; see Section 5). The total fluxes of the optical band are given by black points, and the gray points indicate non-stellar fluxes. The blue shaded regions show the power-law fit of X-ray data. The thin dotted lines show the sensitivity curves for FORCE (100 ks; Nakazawa et al. 2018) and AMEGO (1-year; Moiseev & Amego Team 2017). The data are taken from Dinçer et al. (2018) for A0620-00, Zurita et al. (2004); Hynes et al. (2009) for V404 Cyg, and McClintock et al. (2003); Plotkin et al. (2013) for XTE J1118+480.

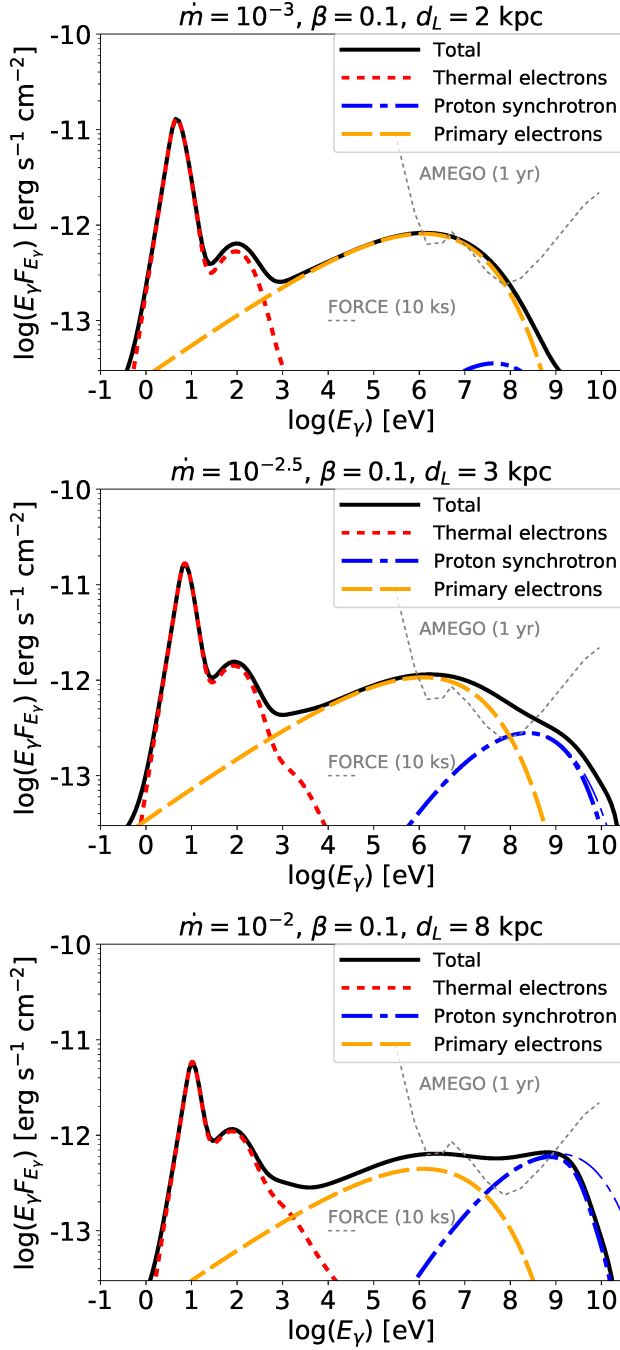


Figure 3. Same as Figure 2, but for hypothetical X-ray binaries with higher values of \dot{m} . The integration time for FORCE sensitivity curves are also changed to 10 ks. In the bottom panel, the thin line represents the intrinsic spectrum at the source, and the thick line is the flux attenuated by $\gamma\gamma$ pair production.

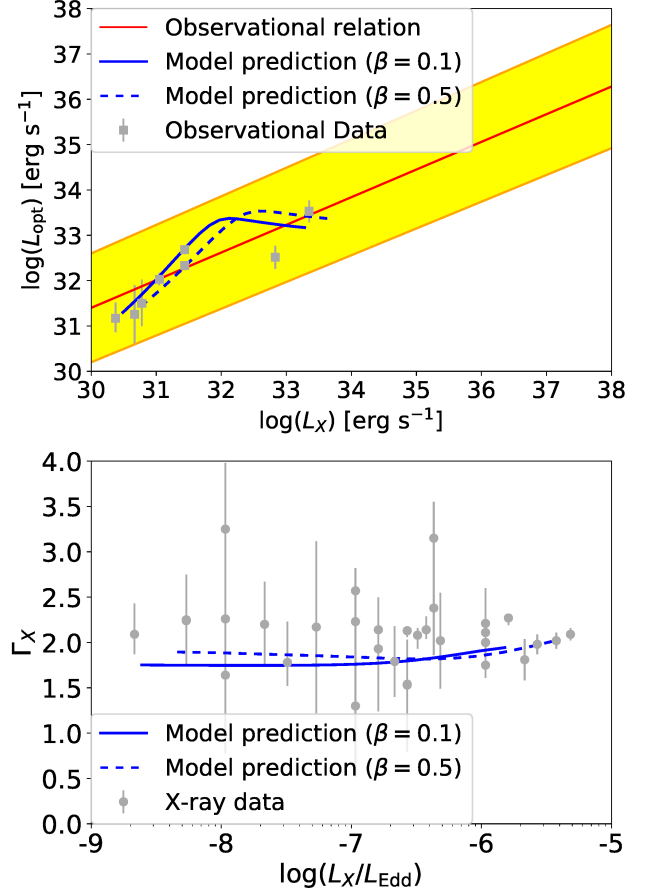


Figure 4. Top panel: $L_{\text{opt}} - L_X$ relation for our QBXB-MAD scenario (solid line) and observations of QBXBs (data points; Russell et al. 2006). The yellow regions indicates the observed $L_{\text{opt}} - L_X$ relation including both quiescent and hard states (Russell et al. 2006). Bottom panel: $\Gamma_X - L_X/L_{\text{Edd}}$ relation in our QBXB-MAD scenario (solid line) and observations (data points; Plotkin et al. 2013).

$\gamma_{e,\text{cl}} = 1$ is realized. The X-ray band lies between the two frequencies where the synchrotron spectrum is given by $E_\gamma L_{E_\gamma} \propto E_\gamma^{(2-s_{\text{inj}})/2}$. The resulting spectra can reproduce the X-ray data of QBXBs within their uncertainty. Future hard X-ray missions, such as FORCE (Nakazawa et al. 2018), will be able to measure the spectrum above 10 keV, which provides a good test of the QBXB-MAD model. Although the spectrum extends to MeV energies, it is too faint to be detected by near future projects, such as e-ASTROGAM (De Angelis et al. 2017), AMEGO (Moiseev & Amego Team 2017), and GRAMS (Aramaki et al. 2020).

The QBXBs in Figure 2 have relatively low mass accretion rates, $\dot{m} \simeq 10^{-5} - 2 \times 10^{-4}$. In our scenario, MADs can be formed in a system with a higher mass accretion rate of $\dot{m} \lesssim 10^{-2}$ (see below for an observa-

tional support). In Figure 3, we show the broadband spectra of hypothetical sources with $10^{-3} \leq \dot{m} \leq 10^{-2}$. The gamma-ray counterpart can be detectable by the MeV satellites up to a few kpc for $\dot{m} \sim 10^{-3}$ and close to 10 kpc for $\dot{m} \sim 10^{-2}$. Such systems might be discovered by current and future X-ray monitoring satellites. Also, known sources may emit detectable MeV gamma-rays during a specific epoch of an outburst, although the time window for the suitable accretion rate is limited.

The multiwavelength observations of QBXBs show the correlation between the optical luminosity, L_{opt} , and X-ray luminosity in the 2-10 keV band, L_X (Russell et al. 2006). In addition, the X-ray observations exhibit that the X-ray photon index, Γ_X , is almost constant for a wide range of the X-ray Eddington ratio of $L_X/L_{\text{Edd}} \lesssim 5 \times 10^{-6}$ (Plotkin et al. 2013)⁶. We calculate photon spectra for various \dot{m} with a fixed $(M_{\text{BH}}/M_{\odot}, \beta) = (10, 0.1)$ and $(10, 0.5)$. The resulting spectra are consistent with the observed relations as shown in Figure 4. These results indicate that the accretion flows in QBXBs are in the MAD regime when $L_X \lesssim 3 \times 10^{33} \text{ erg s}^{-1}$, or $\dot{m} \lesssim 0.01$. In contrast, BH binaries of $L_X/L_{\text{Edd}} > 5 \times 10^{-6}$, i.e. $\dot{m} \gtrsim 0.01$, show an anti-correlation between Γ_X and L_X/L_{Edd} (Wu & Gu 2008). This transition in the $\Gamma_X - L_X/L_{\text{Edd}}$ relation implies that QBXB-MADs no longer exist when $\dot{m} \gtrsim 0.01$.

We note that the free parameters in our calculation are only the mass accretion rate, \dot{m} , and plasma beta, β . We calibrate other parameters (α , \mathcal{R} , ϵ_{dis} , s_{inj} , ϵ_{NT} , η) so that the emission from MADs in radio galaxies can reproduce the GeV gamma-ray data observed by Fermi (Kimura & Toma 2020). We expect that the parameters related to dynamics and non-thermal particle production should be similar in the MADs in radio galaxies and X-ray binaries. The particle acceleration in MADs should occur by magnetic reconnections or stochastic acceleration by turbulence. The characteristics of these processes are determined by the magnetization parameter, σ , and the Alfvén velocity, V_A . Since the temperature and Alfvén velocity are independent of M in the RIAF regime (Kimura et al. 2019a), we expect σ and V_A are similar in radio galaxies and X-ray binaries. Therefore, the parameters for non-thermal particle production should also be similar.

4. CRS FROM QBXB-MADS

⁶ In Plotkin et al. (2013), L_X is defined in the 0.5-10 keV band, while we use L_X of the 2-10 keV band throughout the paper, which results in a factor of ~ 1.9 difference in L_X . Here, we assume the photon index $\Gamma \simeq 2.0$ in the X-ray band.

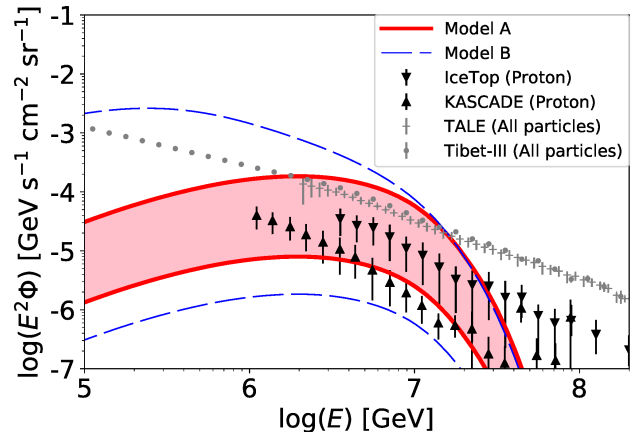


Figure 5. CR spectra predicted by our QBXB-MAD scenario and experimental data. The red and blue lines show the proton CR energy spectra from QBXB-MADs by Method A (population synthesis) and B (X-ray luminosity function), respectively. We use $\beta = 0.1$. The uncertainty range by Method A is shown in the pink shaded region. The experimental data for protons and all-particle CR energy spectra are taken from Apel et al. (2013); Aartsen et al. (2019) and Amenomori et al. (2008); Abbasi et al. (2018), respectively.

Magnetic reconnections in MADs accelerate not only electrons but also protons. CR protons do not have efficient cooling processes in the QBXB-MADs. Significantly high-energy protons can diffusively escape from the system, while lower-energy ones fall to the BH. Equating t_{fall} to t_{esc} , we estimate the critical energy of the escaping protons to be $E_{p,\text{esc}} \approx 3eBV_R R/(c\eta) \simeq 19B_{5.5}V_{R,9}R_7(\eta/5)^{-1} \text{ TeV}$. The maximum proton energy is given by balancing the escape and acceleration, $E_{p,\text{cut}} \approx \sqrt{3eBR\beta_A/\eta} \simeq 0.23B_{5.5}R_7(\beta_A/0.7)(\eta/5)^{-1} \text{ PeV}$. Thus, QBXB-MADs with $\dot{m} \gtrsim 10^{-3}$ can release PeV protons into the interstellar medium (ISM). Magnetic reconnection or stochastic acceleration processes produce both CR protons and CR heavy nuclei. The abundance ratio in the QBXB-MAD should be similar to the solar abundance ratio, and we can neglect the contribution of CR heavy nuclei if the CR injection efficiency is independent of nuclear species.

In order to calculate the CR intensity, we need to estimate the total number of QBXBs. Since this number is uncertain, we utilize two methods. One (Method A) is based on population synthesis. As an analytic estimate, the number of BH X-ray binaries can be represented as

$$\begin{aligned} N_{\text{BHXB}} &\sim \rho_{\text{BH}} f_{\text{bin}} f_{\text{qui}} t_{\text{gal}} \\ &\sim 3 \times 10^4 \rho_{\text{BH}, -2.5} f_{\text{bin}, -1.5} f_{\text{qui}, -1.5} t_{\text{gal}, 10}, \end{aligned} \quad (12)$$

where ρ_{BH} is the BH formation rate, f_{bin} is the fraction of BHs with a low-mass companion, f_{qui} is the

fraction of QBXBs among BH binaries, t_{gal} is the age of our Galaxy, $\rho_{\text{BH},-2.5} = \rho_{\text{BH}}/(10^{-2.5} \text{ yr}^{-1})$, and $t_{\text{gal},10} = t_{\text{gal}}/(10^{10} \text{ yr})$.⁷ This crude estimate is roughly consistent with estimates by binary population synthesis models (e.g., Yungelson et al. 2006). Independently, $N_{\text{BHXB}} \sim 10^3$ is suggested by the event rate of the BH X-ray transients (Corral-Santana et al. 2016) and a recent binary population synthesis model (Shao & Li 2020). Here, we consider that N_{BHXB} ranges from 10^3 to 3×10^4 . We assume a flat \dot{m} distribution in logarithmic space in the range of $\dot{m} = 10^{-5} - 10^{-2}$ for simplicity, although this assumption may be optimistic. QBXB-MADs of $\dot{m} \gtrsim 10^{-3}$ may be rarer than those of $\dot{m} \sim 10^{-4}$.

The other method (Method B) is based on X-ray luminosity functions. In our QBXB-MAD scenario, the X-ray luminosity is well approximated by $L_X \approx 2.6 \times 10^{35} \dot{m} \text{ erg s}^{-1}$, and the X-ray luminosity ranges from $3 \times 10^{30} - 3 \times 10^{33} \text{ erg s}^{-1}$ for $10^{-5} \leq \dot{m} \leq 10^{-2}$. The X-ray luminosity function for $L_X \sim 10^{30} - 10^{34} \text{ erg s}^{-1}$ is dominated by cataclysmic variables (CVs). The luminosity function for CRs per unit stellar mass is given by $dN/d\log_{10}(L_X) \approx K(L_X/L_b)^{1.22}$, where $K = 6.8 \times 10^{-4} M_{\odot}^{-1}$ and $L_b = 1.9 \times 10^{30} \text{ erg s}^{-1}$ (Sazonov et al. 2006). We use the Galactic stellar mass of $M_* = 6 \times 10^{10} M_{\odot}$ (Licquia & Newman 2015) to obtain the total number of CVs in the Milky Way. The RXTE survey identified 24 CVs while 21 objects are unidentified. If all the unidentified sources are QBXB-MADs, the X-ray luminosity function of QBXB-MADs can be as high as 87.5% of that of CVs. This case is regarded as the most optimistic case. On the other hand, the luminosity function of Galactic LMXBs is flat, $dN/d\log_{10}(L_X) \approx 100$, for $10^{35} \text{ erg s}^{-1} < L_X < 10^{37} \text{ erg s}^{-1}$ (Sazonov et al. 2006). As the most pessimistic case, we use the extrapolation of the luminosity function of LMXBs toward lower luminosities.

The differential CR-proton injection rate to the ISM is written as

$$E_p Q_{E_p} \approx \int \frac{E_p^2 N_{E_p}}{t_{\text{diff}}} \frac{dN_{\text{LMBH}}}{d\dot{m}} d\dot{m}. \quad (13)$$

CR protons propagate in the ISM and arrive on Earth. The confinement time in the ISM, t_{conf} , can be provided by the grammage, $X_{\text{esc}} = n_{\text{ISM}} \mu m_p c t_{\text{conf}}$, where n_{ISM} and μ are the number density and mean atomic

mass of the ISM gas, respectively. Based on the measurements of the boron-to-carbon ratio, the grammage is estimated to be $X_{\text{esc}} \simeq 2.0(E_p/250 \text{ GeV})^{-\delta} \text{ g cm}^{-2}$, where $\delta = 0.46$ for $E_p < 250 \text{ GeV}$ and $\delta = 0.33$ for $E_p > 250 \text{ GeV}$ (Adriani et al. 2014; Aguilar et al. 2016; Murase & Fukugita 2019). Then, the CR escape rate from the ISM is estimated to be $E_p U_{E_p} V_{\text{gal}}/t_{\text{conf}} \approx E_p U_{E_p} c M_{\text{gas}}/X_{\text{esc}}$, where U_{E_p} is the differential energy density of CR protons and $M_{\text{gas}} \simeq 8 \times 10^9 M_{\odot}$ is the total gas mass in our Galaxy (Nakanishi & Sofue 2016). This escape rate should balance with the injection rate, and then, we can estimate the CR proton intensity, $\Phi_p = c U_{E_p}/(4\pi E_p)$, to be (Kimura et al. 2018)

$$E_p^2 \Phi_p \approx \frac{E_p Q_{E_p} X_{\text{esc}}}{4\pi M_{\text{gas}}}. \quad (14)$$

Figure 5 depicts the CR proton spectrum from the QBXB-MADs. Our scenario can reproduce the CR proton data around the knee energy within the uncertainty ranges of the experimental data and the total number of QBXB-MADs. The CR composition around the knee is dominated by protons (Telescope Array Collaboration 2020), which is also consistent with our prediction. Galactic SNRs should account for CRs of $\lesssim 10^6 \text{ GeV}$, while other sources, such as binary neutron-star merger remnants (Kimura et al. 2018) or past activities of Sgr A* (Fujita et al. 2017), should be responsible for CRs of $\gtrsim 3 \times 10^7 \text{ GeV}$.

5. DISCUSSION

5.1. Differentiating the emission models for QBXBs

Our QBXB-MAD scenario is distinguishable from the previously proposed scenarios. Moderately magnetized RIAFs, or standard and normal evolution (SANE) scenarios, usually produce bumpy spectra (Esin et al. 1997; Narayan et al. 1997). We calculate the spectra by the SANE-mode RIAFs with one-zone approximation in Figure 2, whose parameters are $(\alpha, \dot{m}/10^{-4}) = (0.2, 0.70), (0.2, 1.0), (0.1, 0.50)$ for A0620-00, V404 Cyg, and XTE J1118+480, respectively. We set $\beta = 3.0$ for all the objects. The SANE-mode RIAFs lead to very soft spectra in the hard X-ray range. On the other hand, MADs produce power-law hard X-ray spectra owing to their non-thermal electrons. FORCE will easily discriminate this feature with 30 – 100 ks integration for A0620-00 and V404 Cyg. XTE J1118+480 demands more time, and the predicted flux by the MAD scenario is close to the design sensitivity. The jet scenarios (Yuan et al. 2005; Pszota et al. 2008) also produce a power-law X-ray spectrum. The time lag of the variability in different wavelengths can be useful to differentiate the scenarios. We expect that the time lag between X-ray and opti-

⁷ If the typical lifetime of companion stars is shorter than the age of our Galaxy, t_{gal} should be replaced by the lifetime of the companion star. Based on BlackCat (Corral-Santana et al. 2016), 15 out of 18 dynamically confirmed BH binaries likely have companions whose lifetimes are longer than the age of the Galaxy, which justifies our estimate.

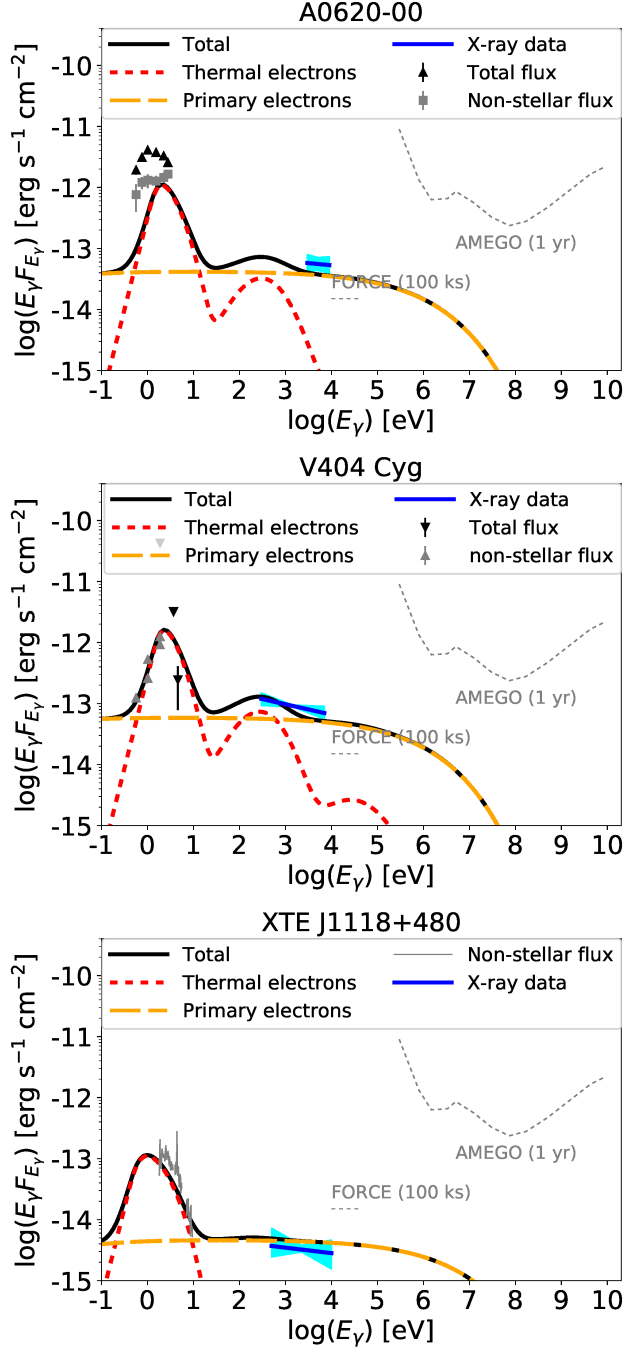


Figure 6. Same as Figure 2, but for $s_{\text{inj}} = 2.0$.

cal bands are shorter than that in the X-ray and radio bands in our QBXB-MAD scenario. This is because the X-ray and optical emissions originate from the same region, while the radio signals originate from jets, and thus, they should follow the variability of X-ray and optical signals with some delay. On the other hand, optical signals are followed by X-ray and radio signals in the jet

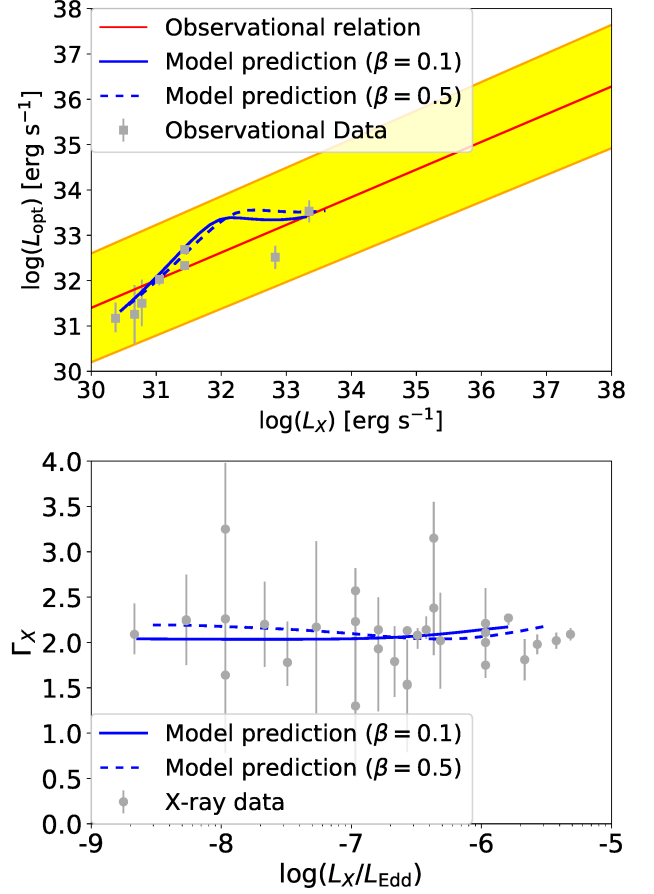


Figure 7. Same as Figure 4, but for $s_{\text{inj}} = 2.0$.

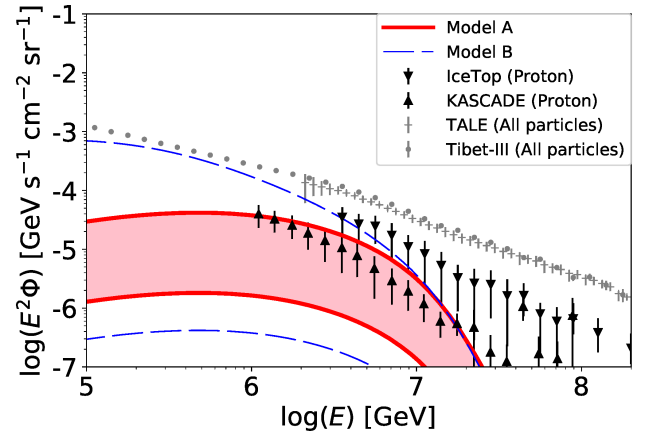


Figure 8. Same as Figure 5, but for $s_{\text{inj}} = 2.0$.

scenario in which optical emission originates from outer accretion disks.

5.2. Cases with higher \dot{m}_o

We focus on the cases with $\dot{m}_o \lesssim 0.01$ in Section 2. For a higher accretion rate of $\dot{m}_o \gtrsim 0.1$, the truncation radius given by Equation (7) shrinks to $R_{\text{trn}} \lesssim (m_p/m_e)R_G$. This leads electron temperature to the trans-relativistic regime, where our assumption is no longer valid. In this situation, the electron temperature can be almost independent of radius, and we can approximate $t_{pe} \propto N_p^{-1} \propto R^{3/2-s_w}$. For the case without outflows, i.e., $s_w = 0$, the dependence of t_{pe} on R is the same with that of t_{fall} , and hence, there is no truncation radius at which t_{pe} and t_{fall} balance each other (Mahadevan & Quataert 1997). With the effect of outflows, the truncation radius for a higher \dot{m}_o is smaller than that for a lower \dot{m}_o . This feature is consistent with the expectation of X-ray transient observations, where the truncation radius is smaller when the X-ray luminosity is higher (Esin et al. 1997).

For a smaller truncation radius of $R_{\text{trn}} \lesssim 100R_G$, the magnetic field amplification by advection is not so drastic, and MADs are not formed instantaneously. Even in this case, the poloidal magnetic field can be accumulated at the horizon as the BH keeps accreting plasmas, and a MAD would eventually be formed if the polarity of the advected poloidal field is aligned for a long time. However, MRI changes the polarity of the field within a few tens of rotation time at the truncation radius (e.g. Suzuki & Inutsuka 2009). Then, the accumulated flux may be canceled out before reaching the MAD state if the truncation radius is small. Such a situation is expected in low-hard states. We leave the quantitative estimate of this phenomenon as a future work, because it has no influence on our discussion as long as we focus on the quiescent state.

5.3. CR production in accretion flows

CRs are highly likely produced in hot components of accretion flows, such as RIAFs or magnetized corone above accretion disks (Liang & Price 1977; Haardt & Maraschi 1991). Observations of high-energy particles provide direct hints of CR production in accretion flows. First, the infrared and X-ray flares of Sgr A* is likely produced by non-thermal electrons accelerated in RIAFs (see e.g., Genzel et al. 2010, for reviews). Also, Fermi-LAT detected GeV gamma-rays from a few radio-quiet active galactic nuclei (AGN) (Wojaczński et al. 2015; Ajello et al. 2020), which may imply the non-thermal particle production in RIAFs or corone. In addition, the hottest spot of the IceCube point source

search of high-energy neutrinos is associated to NGC 1068, a nearby Seyfert galaxy (Aartsen et al. 2020). If this neutrino signal is real, the neutrino flux is much higher than the upper limit of the TeV gamma-rays (Acciari et al. 2019), which indicates that the neutrino source should be “hidden” in gamma-rays (Murase et al. 2016). This implies that the high-energy neutrinos should be produced at the accretion corona rather than the star-burst activities (Inoue et al. 2019; Murase et al. 2020).

From the theoretical view points, the hot components consist of collisionless plasma where the Coulomb relaxation timescale is longer than the viscous dissipation timescales (Takahara & Kusunose 1985; Mahadevan & Quataert 1997; Kimura et al. 2014, 2015; Murase et al. 2020). Accretion flows should be turbulent due to MRI in SANEs (Balbus & Hawley 1991; Stone & Pringle 2001; Machida & Matsumoto 2003; Narayan et al. 2012) or MRTI in MADs (McKinney et al. 2012; White et al. 2019). Then, CRs are naturally accelerated by magnetic reconnections (Hoshino 2015; Kunz et al. 2016; Guo et al. 2020) and/or stochastic acceleration by turbulence (Petrosian 2012; Kimura et al. 2016, 2019b; Zhdankin et al. 2018; Comisso & Sironi 2018). Recent particle-in-cell (PIC) simulations indicated that the particle acceleration is efficient in a strongly magnetized plasma of magnetization parameter $\sigma \approx B^2/(4\pi m_p c^2) > 1$ (Sironi & Spitkovsky 2014; Guo et al. 2016)⁸. Based on GR MHD simulations, MADs can supply reconnection layers of $\sigma \gtrsim 1$ (Ball et al. 2018; Ripperda et al. 2020), and hence, MADs likely produce CRs efficiently. Kimura & Toma (2020) demonstrated that non-thermal particles accelerated in MADs can account for the gamma-ray emissions from nearby radio galaxies.

In our scenario, we assume a hard spectral index of CR protons and electrons, $s_{\text{inj}} = 1.3$. Although magnetic reconnections in solar flares seem to produce a softer CR spectrum (Aschwanden 2002; Ajello et al. 2021), we expect a hard CR spectrum in MADs because magnetic reconnections in highly magnetized plasma ($\sigma > 1$) can efficiently produce non-thermal particles whose spectral index is as hard as $s_{\text{inj}} \sim 1 - 2$ according to PIC simulations (Sironi & Spitkovsky 2014; Guo et al. 2016). Recent results may indicate that the spectrum can be $s_{\text{inj}} \simeq 2$ if non-thermal particles are accelerated to higher energies of $E_i \gtrsim \sigma m_i c^2$ (Petropoulou & Sironi 2018). Our scenario can explain the optical and X-ray data in

⁸ Protons in accretion flows are usually non-relativistic, and we can use the cold plasma limit in the expression of σ .

quiescent states with $s_{\text{inj}} = 2$, as demonstrated in Figures 6 and 7. A softer CR spectrum results in a lower CR proton luminosity at PeV energies. Nevertheless, the resulting CR proton intensity with $s_{\text{inj}} = 2$ is still fairly consistent with the knee-energy CRs as seen in Figure 8.

PIC simulations need to resolve gyration scales of thermal particles, which is several orders of magnitude smaller than the scale of turbulence generated by MRTI. We need to follow the turbulence generated at the largest scale, i.e., the MAD scale, in order to understand the particle acceleration of PeV protons. Since simulations that can follow both the accretion flow and gyration scales are impossible with current facilities, the particle spectra realized in MADs are still uncertain. Further theoretical and observational studies are necessary to unravel the particle accelerations at the vicinity of BHs.

5.4. Relativistic jets from MADs

MADs can launch relativistic jets, whose power is estimated to be $L_j \approx \epsilon_j \dot{m} L_{\text{Edd}} \simeq 1.3 \times 10^{35} \epsilon_{j,-1} \dot{m}_{-3} M_1$, where ϵ_j is the jet production efficiency. For a rapidly spinning BH of $a \approx 1$, where a is the dimensionless spin parameter, $\epsilon_j \approx 1$ can be achieved, while $\epsilon_j \lesssim 0.1$ is more appropriate for a moderate spin parameter of $a \lesssim 0.5$ (Tchekhovskoy et al. 2011; McKinney et al. 2012; Event Horizon Telescope Collaboration et al. 2019). The Hillas energy for protons in the jets can be estimated to be (Hillas 1984; Lemoine & Waxman 2009; Ioka et al. 2017)

$$E_{\text{Hil}} \approx \frac{2e}{\Gamma_j \theta_j} \sqrt{\frac{L_j}{c}} \simeq 1.1 L_{j,35}^{1/2} (\Gamma_j \theta_j)^{-1} \text{ PeV} \quad (15)$$

where Γ_j is the jet Lorentz factor and θ_j is the jet opening angle. Thus, the jets from QBXB-MADs are also potential PeVatrons. The CR luminosity can be estimated to be $L_{\text{CR}}^{\text{jet}} \approx \epsilon_{\text{CR}} L_j$. The ratio of CR luminosities of jets to MADs is estimated to be $L_{\text{CR}}^{\text{jet}}/L_{\text{CR}}^{\text{MAD}} \approx (\epsilon_j \epsilon_{\text{CR}})/(\epsilon_{\text{dis}} \epsilon_{\text{NT}})$. For slowly spinning BHs, we expect $\epsilon_j \epsilon_{\text{CR}} \lesssim 0.01$, which results in $L_{\text{CR}}^{\text{jet}}/L_{\text{CR}}^{\text{MAD}} < 1$. On the other hand, rapidly spinning BHs can achieve $\epsilon_j \epsilon_{\text{CR}} \gtrsim 0.1$, and then, the CR production can be dominated by the jets. Therefore, the spin parameter measurement is crucial to clarify the CR production sites in our scenario.

In hard states, BH X-ray binaries show a correlation between the X-ray luminosity and the radio luminosity, L_R (Merloni et al. 2003; Falcke et al. 2004). This correlation may hold in quiescent states (Rodríguez et al. 2020). In our scenario, the radio emission is produced by jets, while X-rays originate from MADs. Since both

the jet power and the X-ray luminosity from MADs are proportional to the mass accretion rate, it is natural to have the $L_R - L_X$ correlation in QBXB-MADs. The jet production efficiency depends on the spin parameter, and thus, Galactic BHs should have a similar value of a in order to hold a tight correlation. Since the $L_X - L_R$ relation in QBXBs are still not solid, we leave further quantitative discussion as a future work.

BH spins can be measured by the spectral fitting of disk blackbody radiation and the iron fluorescence line broadened by the gravitational redshift (see Reynolds & Nowak 2003; Remillard & McClintock 2006; Done et al. 2007, for reviews). The X-ray data from Cyg X-1 and GX 339-4 can be interpreted with a very high spin of $a \gtrsim 0.9$ (Miller et al. 2008; Gou et al. 2011), whereas other interpretations with lower spin values are possible (e.g. Yamada et al. 2009; Kolehmainen & Done 2010; Kawano et al. 2017). The high resolution X-ray spectroscopy by XRISM (XRISM Science Team 2020) will be able to measure the spin parameters more accurately. These observations should be done during outbursts, because the X-ray fluxes in quiescent states are too low for XRISM to perform spectroscopic observations. On the other hand, gravitational-wave observations revealed that typical binary BHs have a low value of a (Abbott et al. 2020). Although the progenitor of binary BHs should be high-mass X-ray binaries that is a distinct population from low-mass X-ray binaries, this may indicate that stellar mass BHs typically have a low value of a without significant dispersion. In this case, CR proton production in MADs would dominate over that in jets, and QBXB-MADs would likely reproduce the $L_R - L_X$ correlation.

6. SUMMARY

We have discussed the formation scenario of MADs in QBXBs, demonstrated that their broadband photon spectra are consistent with those observed in selected QBXBs, and proposed them as Galactic PeVatrons. In a quiescent state, the mass accretion rate onto a BH is so low that the accretion flow cannot cool efficiently, leading to formation of a RIAF at $\sim 10^4 R_G$. Then, strong outflows produce poloidal fields, and a fast infall will carry the magnetic flux to the vicinity of the BH. We conclude that the accreting plasma with weak poloidal fields ($\beta_p \sim 10^4$) at $R_{\text{trn}} \sim 10^4 R_G$ can form a MAD. Future MHD simulations covering the region from the vicinity of the BH to the truncation radius will be able to test this scenario.

Since the MAD consists of a strongly magnetized collisionless plasma, CR electrons are naturally accelerated via magnetic reconnections or stochastic acceleration by

turbulence. The magnetic reconnections and turbulence cascades also heat up the plasma, and hence, the plasma in the MAD consists of both thermal and non-thermal components. Thermal electrons emit infrared and optical photons via the cyclosynchrotron emission, and CR electrons produce broadband photons from X-rays to MeV gamma-rays by the synchrotron process. We demonstrated that QBXB-MADs can explain both the infrared/optical and X-ray data of the selected BH binaries that have rich data in the quiescent states. QBXB-MADs can also reproduce the observational correlations: $L_X - L_{\text{opt}}$ and $L_X/L_{\text{Edd}} - \Gamma_X$.

CR protons are also accelerated in the QBXB-MADs, and those with TeV-PeV energies can diffusively escape from the system. We have estimated the number density of the QBXBs by two methods, and calculated the CR energy density in the ISM using the grammage and total gas mass in the Galaxy. We found that the CR protons escaping from the QBXB-MADs are fairly consistent with the CR intensity of PeV energies.

In the QBXB-MAD scenario, non-thermal electrons produce a hard photon spectrum in the hard X-ray to MeV gamma-ray ranges. Future hard X-ray satellites,

such as FORCE, will provide a good test of our model. The variability time lags in the different wavelengths (radio/optical/X-rays) can be useful to distinguish our QBXB-MAD model from jet models. Also, if we find an appropriate target with a high accretion rate of $\dot{m} \gtrsim 10^{-3}$, future MeV satellites will be able to detect the QBXB-MADs. These observations are crucial to understand the nature of the QBXBs, especially non-thermal phenomena at the vicinity of BHs. These data, together with the multi-TeV gamma-ray data by future detectors, such as LHAASO (Bai et al. 2019), CTA (Cherenkov Telescope Array Consortium et al. 2019), and SWGO (Albert et al. 2019), will enable us to identify cosmic PeVatrons.

ACKNOWLEDGMENTS

This work is partly supported by JSPS Research Fellowship and KAKENHI No. 19J00198 (S.S.K.), 18J20943 (T.S.), 20K04010, 20H01904 (K.K.), and Hakubi project at Kyoto University (N.K.).

REFERENCES

- Aartsen, M. G., Ackermann, M., Adams, J., et al. 2019, *PhRvD*, 100, 082002, doi: [10.1103/PhysRevD.100.082002](https://doi.org/10.1103/PhysRevD.100.082002)
- Aartsen, M. G., et al. 2020, *Phys. Rev. Lett.*, 124, 051103, doi: [10.1103/PhysRevLett.124.051103](https://doi.org/10.1103/PhysRevLett.124.051103)
- Abbasi, R. U., Abe, M., Abu-Zayyad, T., et al. 2018, *ApJ*, 865, 74, doi: [10.3847/1538-4357/aada05](https://doi.org/10.3847/1538-4357/aada05)
- Abbott, R., et al. 2020. <https://arxiv.org/abs/2010.14527>
- Abeyssekara, A. U., et al. 2020, *Astrophys. J.*, 894, 51, doi: [10.3847/1538-4357/ab8310](https://doi.org/10.3847/1538-4357/ab8310)
- Acciari, V. A., Ansoldi, S., Antonelli, L. A., et al. 2019, *ApJ*, 883, 135, doi: [10.3847/1538-4357/ab3a51](https://doi.org/10.3847/1538-4357/ab3a51)
- Ackermann, M., et al. 2013, *Science*, 339, 807, doi: [10.1126/science.1231160](https://doi.org/10.1126/science.1231160)
- Adriani, O., Barbarino, G. C., Bazilevskaya, G. A., et al. 2014, *ApJ*, 791, 93, doi: [10.1088/0004-637X/791/2/93](https://doi.org/10.1088/0004-637X/791/2/93)
- Aguilar, M., Ali Cavazonza, L., Ambrosi, G., et al. 2016, *Physical Review Letters*, 117, 231102, doi: [10.1103/PhysRevLett.117.231102](https://doi.org/10.1103/PhysRevLett.117.231102)
- Aharonian, F., Yang, R., & de Oña Wilhelmi, E. 2019, *Nature Astron.*, 3, 561, doi: [10.1038/s41550-019-0724-0](https://doi.org/10.1038/s41550-019-0724-0)
- Aharonian, F. A. 2013, *Astroparticle Physics*, 43, 71, doi: [10.1016/j.astropartphys.2012.08.007](https://doi.org/10.1016/j.astropartphys.2012.08.007)
- Ajello, M., Angioni, R., Axelsson, M., et al. 2020, *ApJ*, 892, 105, doi: [10.3847/1538-4357/ab791e](https://doi.org/10.3847/1538-4357/ab791e)
- Ajello, M., Baldini, L., Bastieri, D., et al. 2021, *ApJS*, 252, 13, doi: [10.3847/1538-4365/abd32e](https://doi.org/10.3847/1538-4365/abd32e)
- Albert, A., Alfaro, R., Ashkar, H., et al. 2019, arXiv e-prints, arXiv:1902.08429. <https://arxiv.org/abs/1902.08429>
- Albert, A., Alfaro, R., Alvarez, C., et al. 2020, *ApJL*, 896, L29, doi: [10.3847/2041-8213/ab96cc](https://doi.org/10.3847/2041-8213/ab96cc)
- Amenomori, M., et al. 2008, *Astrophys. J.*, 678, 1165, doi: [10.1086/529514](https://doi.org/10.1086/529514)
- Amenomori, M., Bao, Y. W., Bi, X. J., et al. 2021, *PhRvL*, 126, 141101, doi: [10.1103/PhysRevLett.126.141101](https://doi.org/10.1103/PhysRevLett.126.141101)
- Apel, W. D., Arteaga-Velázquez, J. C., Bekk, K., et al. 2013, *Astroparticle Physics*, 47, 54, doi: [10.1016/j.astropartphys.2013.06.004](https://doi.org/10.1016/j.astropartphys.2013.06.004)
- Aramaki, T., Adrian, P. O. H., Karagiorgi, G., & Odaka, H. 2020, *Astroparticle Physics*, 114, 107, doi: [10.1016/j.astropartphys.2019.07.002](https://doi.org/10.1016/j.astropartphys.2019.07.002)
- Aschwanden, M. J. 2002, *SSRv*, 101, 1, doi: [10.1023/A:1019712124366](https://doi.org/10.1023/A:1019712124366)
- Bai, X., Bi, B. Y., Bi, X. J., et al. 2019, arXiv e-prints, arXiv:1905.02773. <https://arxiv.org/abs/1905.02773>
- Balbus, S. A., & Hawley, J. F. 1991, *ApJ*, 376, 214, doi: [10.1086/170270](https://doi.org/10.1086/170270)
- Ball, D., Özel, F., Psaltis, D., Chan, C.-K., & Sironi, L. 2018, *ApJ*, 853, 184, doi: [10.3847/1538-4357/aaa42f](https://doi.org/10.3847/1538-4357/aaa42f)

- Blandford, R. D., & Begelman, M. C. 1999, *MNRAS*, 303, L1, doi: [10.1046/j.1365-8711.1999.02358.x](https://doi.org/10.1046/j.1365-8711.1999.02358.x)
- Bykov, A. M. 2014, *Astron. Astrophys. Rev.*, 22, 77, doi: [10.1007/s00159-014-0077-8](https://doi.org/10.1007/s00159-014-0077-8)
- Cantrell, A. G., Bailyn, C. D., Orosz, J. A., et al. 2010, *ApJ*, 710, 1127, doi: [10.1088/0004-637X/710/2/1127](https://doi.org/10.1088/0004-637X/710/2/1127)
- Cao, X. 2011, *ApJ*, 737, 94, doi: [10.1088/0004-637X/737/2/94](https://doi.org/10.1088/0004-637X/737/2/94)
- Cherenkov Telescope Array Consortium, Acharya, B. S., Agudo, I., et al. 2019, *Science with the Cherenkov Telescope Array*, doi: [10.1142/10986](https://doi.org/10.1142/10986)
- Chodorowski, M. J., Zdziarski, A. A., & Sikora, M. 1992, *ApJ*, 400, 181, doi: [10.1086/171984](https://doi.org/10.1086/171984)
- Comisso, L., & Sironi, L. 2018, *PhRvL*, 121, 255101, doi: [10.1103/PhysRevLett.121.255101](https://doi.org/10.1103/PhysRevLett.121.255101)
- Cooper, A. J., Gaggero, D., Markoff, S., & Zhang, S. 2020, *MNRAS*, 493, 3212, doi: [10.1093/mnras/staa373](https://doi.org/10.1093/mnras/staa373)
- Corral-Santana, J. M., Casares, J., Muñoz-Darias, T., et al. 2016, *A&A*, 587, A61, doi: [10.1051/0004-6361/201527130](https://doi.org/10.1051/0004-6361/201527130)
- De Angelis, A., Tatischeff, V., Tavani, M., et al. 2017, *Experimental Astronomy*, 44, 25, doi: [10.1007/s10686-017-9533-6](https://doi.org/10.1007/s10686-017-9533-6)
- Diğer, T., Bailyn, C. D., Miller-Jones, J. C. A., Buxton, M., & MacDonald, R. K. D. 2018, *ApJ*, 852, 4, doi: [10.3847/1538-4357/aa9a46](https://doi.org/10.3847/1538-4357/aa9a46)
- Done, C., Gierliński, M., & Kubota, A. 2007, *A&A Rv*, 15, 1, doi: [10.1007/s00159-007-0006-1](https://doi.org/10.1007/s00159-007-0006-1)
- Esin, A. A., McClintock, J. E., & Narayan, R. 1997, *ApJ*, 489, 865, doi: [10.1086/304829](https://doi.org/10.1086/304829)
- Event Horizon Telescope Collaboration, Akiyama, K., Alberdi, A., et al. 2019, *ApJL*, 875, L5, doi: [10.3847/2041-8213/ab0f43](https://doi.org/10.3847/2041-8213/ab0f43)
- Falcke, H., Körding, E., & Markoff, S. 2004, *A&A*, 414, 895, doi: [10.1051/0004-6361:20031683](https://doi.org/10.1051/0004-6361:20031683)
- Fang, K., & Murase, K. 2021, *arXiv e-prints*, arXiv:2104.09491. <https://arxiv.org/abs/2104.09491>
- Fender, R. P., Gallo, E., & Jonker, P. G. 2003, *MNRAS*, 343, L99, doi: [10.1046/j.1365-8711.2003.06950.x](https://doi.org/10.1046/j.1365-8711.2003.06950.x)
- Fujita, Y., Murase, K., & Kimura, S. S. 2017, *JCAP*, 4, 037, doi: [10.1088/1475-7516/2017/04/037](https://doi.org/10.1088/1475-7516/2017/04/037)
- Gandhi, P., Rao, A., Johnson, M. A. C., Paice, J. A., & Maccarone, T. J. 2019, *MNRAS*, 485, 2642, doi: [10.1093/mnras/stz438](https://doi.org/10.1093/mnras/stz438)
- Gelino, D. M., Balman, Ş., Kızıloğlu, Ü., et al. 2006, *ApJ*, 642, 438, doi: [10.1086/500924](https://doi.org/10.1086/500924)
- Genzel, R., Eisenhauer, F., & Gillessen, S. 2010, *Reviews of Modern Physics*, 82, 3121, doi: [10.1103/RevModPhys.82.3121](https://doi.org/10.1103/RevModPhys.82.3121)
- Gou, L., McClintock, J. E., Reid, M. J., et al. 2011, *ApJ*, 742, 85, doi: [10.1088/0004-637X/742/2/85](https://doi.org/10.1088/0004-637X/742/2/85)
- Guépin, C., Rinchiuso, L., Kotera, K., et al. 2018, *JCAP*, 2018, 042, doi: [10.1088/1475-7516/2018/07/042](https://doi.org/10.1088/1475-7516/2018/07/042)
- Guo, F., Liu, Y.-H., Li, X., et al. 2020, *Physics of Plasmas*, 27, 080501, doi: [10.1063/5.0012094](https://doi.org/10.1063/5.0012094)
- Guo, F., Li, X., Li, H., et al. 2016, *ApJL*, 818, L9, doi: [10.3847/2041-8205/818/1/L9](https://doi.org/10.3847/2041-8205/818/1/L9)
- Haardt, F., & Maraschi, L. 1991, *ApJL*, 380, L51, doi: [10.1086/186171](https://doi.org/10.1086/186171)
- Hawley, J. F., Richers, S. A., Guan, X., & Krolik, J. H. 2013, *ApJ*, 772, 102, doi: [10.1088/0004-637X/772/2/102](https://doi.org/10.1088/0004-637X/772/2/102)
- Helder, E. A., Vink, J., Bykov, A. M., et al. 2012, *SSRv*, 173, 369, doi: [10.1007/s11214-012-9919-8](https://doi.org/10.1007/s11214-012-9919-8)
- HESS Collaboration, Abramowski, A., Aharonian, F., et al. 2016, *Nature*, 531, 476, doi: [10.1038/nature17147](https://doi.org/10.1038/nature17147)
- Hillas, A. M. 1984, *ARA&A*, 22, 425, doi: [10.1146/annurev.aa.22.090184.002233](https://doi.org/10.1146/annurev.aa.22.090184.002233)
- Hoshino, M. 2015, *Physical Review Letters*, 114, 061101, doi: [10.1103/PhysRevLett.114.061101](https://doi.org/10.1103/PhysRevLett.114.061101)
- . 2018, *ApJL*, 868, L18, doi: [10.3847/2041-8213/aaef3a](https://doi.org/10.3847/2041-8213/aaef3a)
- Howes, G. G. 2010, *MNRAS*, 409, L104, doi: [10.1111/j.1745-3933.2010.00958.x](https://doi.org/10.1111/j.1745-3933.2010.00958.x)
- Hynes, R. I., Bradley, C. K., Rupen, M., et al. 2009, *MNRAS*, 399, 2239, doi: [10.1111/j.1365-2966.2009.15419.x](https://doi.org/10.1111/j.1365-2966.2009.15419.x)
- Inoue, Y., Khangulyan, D., Inoue, S., & Doi, A. 2019, *ApJ*, 880, 40, doi: [10.3847/1538-4357/ab2715](https://doi.org/10.3847/1538-4357/ab2715)
- Ioka, K., Matsumoto, T., Teraki, Y., Kashiya, K., & Murase, K. 2017, *MNRAS*, 470, 3332, doi: [10.1093/mnras/stx1337](https://doi.org/10.1093/mnras/stx1337)
- Kafexhiu, E., Aharonian, F., Taylor, A. M., & Vila, G. S. 2014, *PhRvD*, 90, 123014, doi: [10.1103/PhysRevD.90.123014](https://doi.org/10.1103/PhysRevD.90.123014)
- Kawano, T., Done, C., Yamada, S., et al. 2017, *PASJ*, 69, 36, doi: [10.1093/pasj/psx009](https://doi.org/10.1093/pasj/psx009)
- Kawazura, Y., Barnes, M., & Schekochihin, A. A. 2019, *Proceedings of the National Academy of Science*, 116, 771, doi: [10.1073/pnas.1812491116](https://doi.org/10.1073/pnas.1812491116)
- Khargharia, J., Froning, C. S., & Robinson, E. L. 2010, *ApJ*, 716, 1105, doi: [10.1088/0004-637X/716/2/1105](https://doi.org/10.1088/0004-637X/716/2/1105)
- Khargharia, J., Froning, C. S., Robinson, E. L., & Gelino, D. M. 2013, *AJ*, 145, 21, doi: [10.1088/0004-6256/145/1/21](https://doi.org/10.1088/0004-6256/145/1/21)
- Kimura, S. S., Murase, K., & Mészáros, P. 2018, *ApJ*, 866, 51, doi: [10.3847/1538-4357/aadc0a](https://doi.org/10.3847/1538-4357/aadc0a)
- . 2019a, *PhRvD*, 100, 083014, doi: [10.1103/PhysRevD.100.083014](https://doi.org/10.1103/PhysRevD.100.083014)
- Kimura, S. S., Murase, K., & Mészáros, P. 2020. <https://arxiv.org/abs/2005.01934>
- Kimura, S. S., Murase, K., & Toma, K. 2015, *ApJ*, 806, 159, doi: [10.1088/0004-637X/806/2/159](https://doi.org/10.1088/0004-637X/806/2/159)

- Kimura, S. S., & Toma, K. 2020, *ApJ*, 905, 178, doi: [10.3847/1538-4357/abc343](https://doi.org/10.3847/1538-4357/abc343)
- Kimura, S. S., Toma, K., Suzuki, T. K., & Inutsuka, S.-i. 2016, *ApJ*, 822, 88, doi: [10.3847/0004-637X/822/2/88](https://doi.org/10.3847/0004-637X/822/2/88)
- Kimura, S. S., Toma, K., & Takahara, F. 2014, *ApJ*, 791, 100, doi: [10.1088/0004-637X/791/2/100](https://doi.org/10.1088/0004-637X/791/2/100)
- Kimura, S. S., Tomida, K., & Murase, K. 2019b, *MNRAS*, 485, 163, doi: [10.1093/mnras/stz329](https://doi.org/10.1093/mnras/stz329)
- Kolehmainen, M., & Done, C. 2010, *MNRAS*, 406, 2206, doi: [10.1111/j.1365-2966.2010.16835.x](https://doi.org/10.1111/j.1365-2966.2010.16835.x)
- Kunz, M. W., Stone, J. M., & Quataert, E. 2016, *Physical Review Letters*, 117, 235101, doi: [10.1103/PhysRevLett.117.235101](https://doi.org/10.1103/PhysRevLett.117.235101)
- Lemoine, M., & Waxman, E. 2009, *JCAP*, 11, 009, doi: [10.1088/1475-7516/2009/11/009](https://doi.org/10.1088/1475-7516/2009/11/009)
- Liang, E. P. T., & Price, R. H. 1977, *ApJ*, 218, 247, doi: [10.1086/155677](https://doi.org/10.1086/155677)
- Licquia, T. C., & Newman, J. A. 2015, *ApJ*, 806, 96, doi: [10.1088/0004-637X/806/1/96](https://doi.org/10.1088/0004-637X/806/1/96)
- Liska, M., Tchekhovskoy, A., & Quataert, E. 2020, *MNRAS*, 494, 3656, doi: [10.1093/mnras/staa955](https://doi.org/10.1093/mnras/staa955)
- Liu, R.-Y., & Wang, X.-Y. 2021, arXiv e-prints, arXiv:2104.05609. <https://arxiv.org/abs/2104.05609>
- Machida, M., & Matsumoto, R. 2003, *ApJ*, 585, 429, doi: [10.1086/346070](https://doi.org/10.1086/346070)
- Mahadevan, R. 1997, *ApJ*, 477, 585, doi: [10.1086/303727](https://doi.org/10.1086/303727)
- Mahadevan, R., Narayan, R., & Yi, I. 1996, *ApJ*, 465, 327, doi: [10.1086/177422](https://doi.org/10.1086/177422)
- Mahadevan, R., & Quataert, E. 1997, *ApJ*, 490, 605
- Manmoto, T., Mineshige, S., & Kusunose, M. 1997, *ApJ*, 489, 791
- McClintock, J. E., Narayan, R., Garcia, M. R., et al. 2003, *ApJ*, 593, 435, doi: [10.1086/376406](https://doi.org/10.1086/376406)
- McKinney, J. C., Tchekhovskoy, A., & Blandford, R. D. 2012, *MNRAS*, 423, 3083, doi: [10.1111/j.1365-2966.2012.21074.x](https://doi.org/10.1111/j.1365-2966.2012.21074.x)
- Merloni, A., Heinz, S., & di Matteo, T. 2003, *MNRAS*, 345, 1057, doi: [10.1046/j.1365-2966.2003.07017.x](https://doi.org/10.1046/j.1365-2966.2003.07017.x)
- Miller, J. M., Reynolds, C. S., Fabian, A. C., et al. 2008, *ApJL*, 679, L113, doi: [10.1086/589446](https://doi.org/10.1086/589446)
- Miller-Jones, J. C. A., Jonker, P. G., Dhawan, V., et al. 2009, *ApJL*, 706, L230, doi: [10.1088/0004-637X/706/2/L230](https://doi.org/10.1088/0004-637X/706/2/L230)
- Moiseev, A., & Amego Team. 2017, *International Cosmic Ray Conference*, 301, 798
- Murase, K., & Fukugita, M. 2019, *PhRvD*, 99, 063012, doi: [10.1103/PhysRevD.99.063012](https://doi.org/10.1103/PhysRevD.99.063012)
- Murase, K., Guetta, D., & Ahlers, M. 2016, *Phys. Rev. Lett.*, 116, 071101, doi: [10.1103/PhysRevLett.116.071101](https://doi.org/10.1103/PhysRevLett.116.071101)
- Murase, K., Kimura, S. S., & Meszaros, P. 2020, *Phys. Rev. Lett.*, 125, 011101, doi: [10.1103/PhysRevLett.125.011101](https://doi.org/10.1103/PhysRevLett.125.011101)
- Murase, K., & Nagataki, S. 2006, *PhRvD*, 73, 063002, doi: [10.1103/PhysRevD.73.063002](https://doi.org/10.1103/PhysRevD.73.063002)
- Nakanishi, H., & Sofue, Y. 2016, *PASJ*, 68, 5, doi: [10.1093/pasj/psv108](https://doi.org/10.1093/pasj/psv108)
- Nakazawa, K., Mori, K., Tsuru, T. G., et al. 2018, in *Society of Photo-Optical Instrumentation Engineers (SPIE) Conference Series*, Vol. 10699, *Space Telescopes and Instrumentation 2018: Ultraviolet to Gamma Ray*, ed. J.-W. A. den Herder, S. Nikzad, & K. Nakazawa, 106992D, doi: [10.1117/12.2309344](https://doi.org/10.1117/12.2309344)
- Narayan, R., Barret, D., & McClintock, J. E. 1997, *ApJ*, 482, 448, doi: [10.1086/304134](https://doi.org/10.1086/304134)
- Narayan, R., Sądowski, A., Penna, R. F., & Kulkarni, A. K. 2012, *MNRAS*, 426, 3241, doi: [10.1111/j.1365-2966.2012.22002.x](https://doi.org/10.1111/j.1365-2966.2012.22002.x)
- Narayan, R., & Yi, I. 1994, *ApJL*, 428, L13, doi: [10.1086/187381](https://doi.org/10.1086/187381)
- . 1995, *ApJ*, 452, 710, doi: [10.1086/176343](https://doi.org/10.1086/176343)
- Narayan, R., Yi, I., & Mahadevan, R. 1995, *Nature*, 374, 623, doi: [10.1038/374623a0](https://doi.org/10.1038/374623a0)
- Nemmen, R. S., Storch-Bergmann, T., & Eracleous, M. 2014, *MNRAS*, 438, 2804, doi: [10.1093/mnras/stt2388](https://doi.org/10.1093/mnras/stt2388)
- Ohira, Y., Kisaka, S., & Yamazaki, R. 2018, *MNRAS*, 478, 926, doi: [10.1093/mnras/sty1159](https://doi.org/10.1093/mnras/sty1159)
- Ohsuga, K., & Mineshige, S. 2011, *ApJ*, 736, 2, doi: [10.1088/0004-637X/736/1/2](https://doi.org/10.1088/0004-637X/736/1/2)
- Orosz, J. A., Bailyn, C. D., Remillard, R. A., McClintock, J. E., & Foltz, C. B. 1994, *ApJ*, 436, 848, doi: [10.1086/174962](https://doi.org/10.1086/174962)
- Petropoulou, M., & Sironi, L. 2018, *MNRAS*, 481, 5687, doi: [10.1093/mnras/sty2702](https://doi.org/10.1093/mnras/sty2702)
- Petrosian, V. 2012, *SSRv*, 173, 535, doi: [10.1007/s11214-012-9900-6](https://doi.org/10.1007/s11214-012-9900-6)
- Plotkin, R. M., Gallo, E., & Jonker, P. G. 2013, *ApJ*, 773, 59, doi: [10.1088/0004-637X/773/1/59](https://doi.org/10.1088/0004-637X/773/1/59)
- Plotkin, R. M., Gallo, E., Markoff, S., et al. 2015, *MNRAS*, 446, 4098, doi: [10.1093/mnras/stu2385](https://doi.org/10.1093/mnras/stu2385)
- Pszota, G., Zhang, H., Yuan, F., & Cui, W. 2008, *MNRAS*, 389, 423, doi: [10.1111/j.1365-2966.2008.13587.x](https://doi.org/10.1111/j.1365-2966.2008.13587.x)
- Quataert, E., & Narayan, R. 1999, *ApJ*, 520, 298, doi: [10.1086/307439](https://doi.org/10.1086/307439)
- Remillard, R. A., & McClintock, J. E. 2006, *ARA&A*, 44, 49, doi: [10.1146/annurev.astro.44.051905.092532](https://doi.org/10.1146/annurev.astro.44.051905.092532)
- Ressler, S. M., White, C. J., Quataert, E., & Stone, J. M. 2020, *ApJL*, 896, L6, doi: [10.3847/2041-8213/ab9532](https://doi.org/10.3847/2041-8213/ab9532)
- Reynolds, C. S., & Nowak, M. A. 2003, *PhR*, 377, 389, doi: [10.1016/S0370-1573\(02\)00584-7](https://doi.org/10.1016/S0370-1573(02)00584-7)

- Ripperda, B., Bacchini, F., & Philippov, A. A. 2020, *ApJ*, 900, 100, doi: [10.3847/1538-4357/ababab](https://doi.org/10.3847/1538-4357/ababab)
- Rodriguez, J., Urquhart, R., Plotkin, R. M., et al. 2020, *ApJ*, 889, 58, doi: [10.3847/1538-4357/ab5db5](https://doi.org/10.3847/1538-4357/ab5db5)
- Rowan, M. E., Sironi, L., & Narayan, R. 2017, *ApJ*, 850, 29, doi: [10.3847/1538-4357/aa9380](https://doi.org/10.3847/1538-4357/aa9380)
- Russell, D. M., Fender, R. P., Hynes, R. I., et al. 2006, *MNRAS*, 371, 1334, doi: [10.1111/j.1365-2966.2006.10756.x](https://doi.org/10.1111/j.1365-2966.2006.10756.x)
- Sazonov, S., Revnivtsev, M., Gilfanov, M., Churazov, E., & Sunyaev, R. 2006, *A&A*, 450, 117, doi: [10.1051/0004-6361:20054297](https://doi.org/10.1051/0004-6361:20054297)
- Sądowski, A., Narayan, R., Penna, R., & Zhu, Y. 2013, *MNRAS*, 436, 3856, doi: [10.1093/mnras/stt1881](https://doi.org/10.1093/mnras/stt1881)
- Schure, K. M., Bell, A. R., O’C Drury, L., & Bykov, A. M. 2012, *SSRv*, 173, 491, doi: [10.1007/s11214-012-9871-7](https://doi.org/10.1007/s11214-012-9871-7)
- Shakura, N. I., & Sunyaev, R. A. 1973, *A&A*, 24, 337
- Shao, Y., & Li, X.-D. 2020, *ApJ*, 898, 143, doi: [10.3847/1538-4357/aba118](https://doi.org/10.3847/1538-4357/aba118)
- Sironi, L., & Spitkovsky, A. 2014, *ApJ*, 783, L21, doi: [10.1088/2041-8205/783/1/L21](https://doi.org/10.1088/2041-8205/783/1/L21)
- Stepney, S., & Guilbert, P. W. 1983, *MNRAS*, 204, 1269, doi: [10.1093/mnras/204.4.1269](https://doi.org/10.1093/mnras/204.4.1269)
- Stone, J. M., & Pringle, J. E. 2001, *MNRAS*, 322, 461, doi: [10.1046/j.1365-8711.2001.04138.x](https://doi.org/10.1046/j.1365-8711.2001.04138.x)
- Suzuki, T. K., & Inutsuka, S.-i. 2009, *ApJL*, 691, L49, doi: [10.1088/0004-637X/691/1/L49](https://doi.org/10.1088/0004-637X/691/1/L49)
- Takahara, F., & Kusunose, M. 1985, *Progress of Theoretical Physics*, 73, 1390, doi: [10.1143/PTP.73.1390](https://doi.org/10.1143/PTP.73.1390)
- Tchekhovskoy, A., Metzger, B. D., Giannios, D., & Kelley, L. Z. 2014, *MNRAS*, 437, 2744, doi: [10.1093/mnras/stt2085](https://doi.org/10.1093/mnras/stt2085)
- Tchekhovskoy, A., Narayan, R., & McKinney, J. C. 2011, *MNRAS*, 418, L79, doi: [10.1111/j.1745-3933.2011.01147.x](https://doi.org/10.1111/j.1745-3933.2011.01147.x)
- Telescope Array Collaboration. 2020, arXiv e-prints, arXiv:2012.10372. <https://arxiv.org/abs/2012.10372>
- Tetarenko, B. E., Sivakoff, G. R., Heinke, C. O., & Gladstone, J. C. 2016, *ApJS*, 222, 15, doi: [10.3847/0067-0049/222/2/15](https://doi.org/10.3847/0067-0049/222/2/15)
- Tibet AS γ Collaboration, Amenomori, M., Bao, Y. W., et al. 2021, *Nature Astronomy*, doi: [10.1038/s41550-020-01294-9](https://doi.org/10.1038/s41550-020-01294-9)
- White, C. J., Quataert, E., & Gammie, C. F. 2020, *ApJ*, 891, 63, doi: [10.3847/1538-4357/ab718e](https://doi.org/10.3847/1538-4357/ab718e)
- White, C. J., Stone, J. M., & Quataert, E. 2019, *ApJ*, 874, 168, doi: [10.3847/1538-4357/ab0c0c](https://doi.org/10.3847/1538-4357/ab0c0c)
- Wojaczyński, R., Niedźwiecki, A., Xie, F.-G., & Szanecki, M. 2015, *A&A*, 584, A20, doi: [10.1051/0004-6361/201526621](https://doi.org/10.1051/0004-6361/201526621)
- Wu, Q., & Gu, M. 2008, *ApJ*, 682, 212, doi: [10.1086/588187](https://doi.org/10.1086/588187)
- XRISM Science Team. 2020, arXiv e-prints, arXiv:2003.04962. <https://arxiv.org/abs/2003.04962>
- Yamada, S., Makishima, K., Uehara, Y., et al. 2009, *ApJL*, 707, L109, doi: [10.1088/0004-637X/707/2/L109](https://doi.org/10.1088/0004-637X/707/2/L109)
- Yuan, F., Cui, W., & Narayan, R. 2005, *ApJ*, 620, 905, doi: [10.1086/427206](https://doi.org/10.1086/427206)
- Yuan, F., Gan, Z., Narayan, R., et al. 2015, *ApJ*, 804, 101, doi: [10.1088/0004-637X/804/2/101](https://doi.org/10.1088/0004-637X/804/2/101)
- Yuan, F., & Narayan, R. 2014, *ARA&A*, 52, 529, doi: [10.1146/annurev-astro-082812-141003](https://doi.org/10.1146/annurev-astro-082812-141003)
- Yuan, F., Quataert, E., & Narayan, R. 2003, *ApJ*, 598, 301, doi: [10.1086/378716](https://doi.org/10.1086/378716)
- Yungelson, L. R., Lasota, J. P., Nelemans, G., et al. 2006, *A&A*, 454, 559, doi: [10.1051/0004-6361:20064984](https://doi.org/10.1051/0004-6361:20064984)
- Zamaninasab, M., Clausen-Brown, E., Savolainen, T., & Tchekhovskoy, A. 2014, *Nature*, 510, 126, doi: [10.1038/nature13399](https://doi.org/10.1038/nature13399)
- Zdziarski, A. A., Sikora, M., Pjanka, P., & Tchekhovskoy, A. 2015, *MNRAS*, 451, 927, doi: [10.1093/mnras/stv986](https://doi.org/10.1093/mnras/stv986)
- Zenitani, S., & Hoshino, M. 2001, *ApJ*, 562, L63, doi: [10.1086/337972](https://doi.org/10.1086/337972)
- Zhdankin, V., Uzdensky, D. A., Werner, G. R., & Begelman, M. C. 2018, *ApJL*, 867, L18, doi: [10.3847/2041-8213/aae88c](https://doi.org/10.3847/2041-8213/aae88c)
- Zurita, C., Casares, J., Hynes, R. I., et al. 2004, *MNRAS*, 352, 877, doi: [10.1111/j.1365-2966.2004.07979.x](https://doi.org/10.1111/j.1365-2966.2004.07979.x)